Rare earth elements and neodymium and strontium isotopic constraints on provenance switch and post-depositional alteration of fossiliferous Ediacaran and lowermost Cambrian strata from Arctic Norway

Guido Meinhold [a,b,*], Matthias Willbold [c], Volker Karius [b], Sören Jensen [d], Heda Agić [e,f], Jan Ove R. Ebbestad [g], Teodoro Palacios [d], Anette E.S. Högström [h], Magne Høyberget [i], Wendy L. Taylor [j]

[a] *Institute of Geology, TU Bergakademie Freiberg, Bernhard-von-Cotta-Straße 2, D-09599 Freiberg, Germany*
[b] *Department of Sedimentology and Environmental Geology, University of Göttingen, Goldschmidtstraße 3, D-37077 Göttingen, Germany*
[c] *Department of Geochemistry and Isotope Geology, University of Göttingen, Goldschmidtstraße 1, D-37077 Göttingen, Germany*
[d] *Área de Paleontología, Facultad de Ciencias, Universidad de Extremadura, Avenida de Física, E-06006 Badajoz, Spain*
[e] *Department of Earth Science, University of California at Santa Barbara, Santa Barbara, CA 93106, USA*
[f] *Department of Earth Sciences, Durham University, Lower Mountjoy, Durham DH1 3LE, UK*
[g] *Museum of Evolution, Uppsala University, Norbyvägen 16, SE 752 36 Uppsala, Sweden*
[h] *Arctic University Museum of Norway, UiT – The Arctic University of Norway, N-9037 Tromsø, Norway*
[i] *Rennesveien 14, N-4513 Mandal, Norway*
[j] *Department of Geological Sciences, University of Cape Town, Private Bag X3, Rondebosch 7701, South Africa*

ARTICLE INFO

ABSTRACT

The Digermulen Peninsula in northeastern Finnmark, Arctic Norway, comprises one of the most complete Ediacaran–Cambrian transitions worldwide with a nearly continuous record of micro- and macrofossils from the interval of the diversification of complex life. Here, we report on the provenance and post-depositional alteration of argillaceous mudstones from the Digermulen Peninsula using rare earth elements and Sm–Nd and Rb–Sr isotopic systematics to provide an environmental context and better understand this important transition in Earth's history. The studied sections comprise a mid-Ediacaran glacial–interglacial cycle, including the Nyborg Formation (ca. 590 Ma) and Mortensnes Formation (related to the ca. 580 Ma-old Gaskiers glaciation), and the Stáhpogieddi Formation (ca. 560–537 Ma), which yields Ediacara-type fossils in the Indreelva Member and contains the Ediacaran–Cambrian boundary interval in the Manndrapselva Member and basal part of the informal Lower Breidvika member (ca. 537–530 Ma). Three sample groups, (1) Nyborg and Mortensnes formations, (2) the lowermost five samples from the Indreelva Member and (3) the remaining samples from the Indreelva as well as from the Manndrapselva and Lower Breidvika members, can be distinguished, belonging to distinct depositional units. All samples have negative $\varepsilon_{Nd}(T)$ values (−6.00 to − 21.04) indicating a dominant input of terrigenous detritus with an old continental crust affinity. Significant shifts in Sm–Nd isotope values are related to changes in the sediment source, i.e. Svecofennian province vs Karelian province vs Svecofennian province plus in addition likely some juvenile (late Neoproterozoic volcanic) material, and probably reflect palaeotectonic reorganisation along the Iapetus-facing margin of Baltica. The combined Rb–Sr isotopic data of all samples yield an errorchron age of about 430 Ma reflecting the resetting of the Rb–Sr whole-rock isotope systems of the mudstones during the Scandian tectono-metamorphic event in the Gaissa Nappe Complex of Finnmark. Preservation of palaeopascichnids coincides with the sedimentation regimes of sample groups 2 and 3 while other Ediacara-type fossils, e.g. *Aspidella*-type and frondose forms, are limited to the sample group 3. Our results are similar to those of earlier studies from the East European Platform in suggesting oxic seafloor conditions during the late Ediacaran.

1. Introduction

The Ediacaran Period is an important interval of Earth's history when metazoans started to flourish following the 'Snowball Earth' glaciations (Cunningham et al., 2017; Wood et al., 2019, and references therein). To better understand the depositional environment that may have benefited or hindered the evolution of this early complex life, the Ediacaran sedimentary successions are studied in great detail worldwide, through whole-rock geochemical and isotopic studies, among other proxies. Geochemical and isotopic studies of siliciclastic sedimentary rocks are critical for deciphering the age and composition of rock lithologies in the source area and hence for palaeotectonic reconstructions. Fine-grained siliciclastic sediment (mud) or sedimentary rock (mudstones, according to the nomenclature of Lazar et al., 2015) is thought to be the most appropriate lithology for such studies because the detritus is thoroughly mixed during weathering processes and transport of sediments, and chemical modification of the sediment during deposition and burial diagenesis is less pronounced than in coarser sediment (Allègre and Rousseau, 1984; Condie, 1991; Cullers, 1995). Thus, they provide a representative sampling of the provenance, i.e. the exposed upper continental crustal rocks at the time of deposition of the sediment (Taylor and McLennan, 1985).

Rare earth elements (REEs), also called lanthanides, are widely used as tracers for redox changes and sedimentary provenance of fine-grained sedimentary rocks (e.g., McLennan, 1989; McLennan et al., 1990, 1993). The REEs are a group of chemically coherent elements, comprising lanthanum (La) to lutetium (Lu), that all exist in a trivalent oxidation state except for cerium (Ce) and europium (Eu) which are redox sensitive and may take different valence states depending on the oxygen fugacity (fO$_2$) (Elderfield and Greaves, 1982). At high fO$_2$, Ce can be in the tetravalent oxidation state (Ce^{4+}), while under low fO$_2$, Eu can be in the divalent oxidation state (Eu^{2+}) (Elderfield and Greaves, 1982; Gao and Wedepohl, 1995). Besides the REEs, also Sm–Nd whole-rock isotope systematics have proved to be a valuable tool for unravelling the provenance of fine-grained sedimentary rocks (McCulloch and Wasserburg, 1978; O'Nions et al., 1983; Allègre and Rousseau, 1984; Goldstein et al., 1984; Nelson and DePaolo, 1988; McLennan and Hemming, 1992; Bock et al., 1994; Roy et al., 2007; Awasthi et al., 2018). This is because Sm/Nd fractionation occurs largely during extraction of melts from the mantle to the crust (McCulloch and Wasserburg, 1978; DePaolo, 1981), whereas processes such as erosion, weathering, transport, sedimentation, diagenesis and metamorphism do not fractionate Sm from Nd appreciably. Both elements belong to the light REE (LREE include La, Ce, Pr, Nd, Pm, and Sm), and thus the Nd isotope signature of the detritus carried into sedimentary basins reflects the average lithology and average 'crustal residence age' of the eroded source rocks (e.g., McCulloch and Wasserburg, 1978; Allègre and Rousseau, 1984; Goldstein et al., 1984; McLennan and Hemming, 1992; Roy et al., 2007; Awasthi et al., 2018). Changes in the isotope composition and crustal residence ages throughout a stratigraphic section are utilized to unravel prominent changes in provenance, reflecting continent-scale tectonic reorganisation. Crustal residence ages are often referred to as model ages (Arndt and Goldstein, 1987). It should be noted that the Nd isotope system may be reset due to mobility of LREE under certain circumstances during diagenesis (Awwiller and Mack, 1991; Milodowski and Zalasiewicz, 1991; Bock et al., 1994, 1998). Regardless of this observation, it is still possible to extract important provenance information from Sm–Nd isotopic data (Bock et al., 1998).

^{87}Rb–^{87}Sr whole-rock isotopic data are also informative to study past depositional settings, although the data are less reliable for provenance studies because the Sr isotope values (e.g., ^{87}Sr/^{86}Sr) can be modified during fluvial transport (Awasthi et al., 2018) and diagenesis (McCulloch and Wasserburg, 1978; Ohr et al., 1991). Apart from that, already low-grade metamorphism commonly resets the ^{87}Rb–^{87}Sr whole-rock isotope system, and thus, the ^{87}Rb–^{87}Sr whole-rock isotope method is useful to determine the age of metamorphic overprint (Compston and

Pidgeon, 1962; Gebauer and Grünenfelder, 1974) but is inadequate for finding the composition and age of the source area of metasedimentary rocks. ^{87}Rb–^{87}Sr isotopic analysis were carried out on upper Neoproterozoic sedimentary rocks from the Varanger Peninsula in Finnmark (Pringle, 1973; Gorokhov et al., 2001) but have not yet been performed on sedimentary rocks from the adjacent Digermulen Peninsula to the west (Figs. 1, 2).

Here, we apply for the first time ^{147}Sm–^{143}Nd and ^{87}Rb–^{87}Sr whole-rock isotopic analyses to low-grade metamorphosed mudstones from the Digermulen Peninsula in northern Norway (Figs. 1, 2), in order to understand sediment composition, provenance and post-depositional alteration. This area is the only fossiliferous site in Scandinavia with sedimentation across the Ediacaran–Cambrian transition without a significant hiatus (Högström et al., 2013) (Fig. 3). Furthermore, it is the only locality in Scandinavia where Ediacara biota fossils have been found (Farmer et al., 1992; Högström et al., 2013; Jensen et al., 2018a,b) (Fig. 4), and a goal of this work is to understand the way these fossils are preserved as well as the conditions they were deposited in. Our ^{147}Sm–^{143}Nd isotopic data provide the first constraints on provenance changes across a glacial–interglacial cycle and the fossil-bearing Ediacaran–Cambrian boundary interval in Scandinavia. Results from the ^{87}Rb–^{87}Sr whole-rock isochron method (this study) are compared with previously obtained ages for the metamorphic overprint based on fine-fraction ^{40}K–^{40}Ar (Meinhold et al., 2019b) and in situ ^{238,235}U–^{206,207}Pb calcite data (Meinhold et al., 2020). Finally, we explore how redox-sensitive elements (primarily Ce) in the Digermulen succession relate to the stratigraphical distribution of palaeopascichnids and Ediacara-type fossils. The appearance of probable metazoan macroscopic fossils of the Ediacara biota at approximately 575 Ma, as well as later Ediacaran diversity changes and extinctions, have been linked to the late Neoproterozoic rise in seawater oxygenation and to Ediacaran anoxic events (e.g., Sahoo et al., 2016; Evans et al., 2018; Zhang et al., 2019; Rooney et al., 2020; Shi et al., 2022). The data from the continuous Digermulen succession cast further light on this discussion.

2. Geological setting

2.1. Regional geology

The sedimentary succession of the Digermulen Peninsula belongs to the Lower Allochthon Gaissa Nappe Complex of the Caledonides of Finnmark (Rice, 2014) (Fig. 1). The rocks belong to the Cryogenian to lower Cambrian Vestertana Group, comprising in ascending order the Smalfjorden, Nyborg, Mortensnes, Stáhpogieddi and Breidvika formations (Reading, 1965; Reading and Walker, 1966; Banks et al., 1971) (Fig. 2, 3). The glacial deposits of the Smalfjorden and Mortensnes formations (e.g., Reading and Walker, 1966; Banks et al., 1971), separated by the interglacial Nyborg Formation (Reading and Walker, 1966), are collectively known as the Varanger Ice Age (e.g., Nystuen, 1985). The Smalfjorden Formation has been correlated with glaciogenic deposits of the Marinoan glaciation (e.g., Rice et al., 2011) of Cryogenian age (ca. 645–635 Ma, Rooney et al., 2015; Shields-Zhou et al., 2016). The Mortensnes Formation on the other hand has been correlated with those of the Ediacaran Gaskiers glaciation (e.g., Rice et al., 2011), which was likely of short duration (ca. 580 Ma, Pu et al., 2016). The age of these glacial deposits has recently been challenged by Kumpulainen et al. (2021), who suggest that all Neoproterozoic glacial successions in Scandinavia probably belong to the Marinoan glaciation, which is a global Snowball Earth glacial episode. Kumpulainen et al. (2021) base their interpretation on cross-cutting relationships between glacial successions and a ca. 596 Ma-old mafic igneous dyke in the Särv Nappe of the central Scandinavian Caledonides in Jämtland, west-central Sweden. A Marinoan age may be true for the study area in Jämtland. However, as long as no reliable and unequivocal geochronological data are available from Finnmark and independent proof that the age constraint from
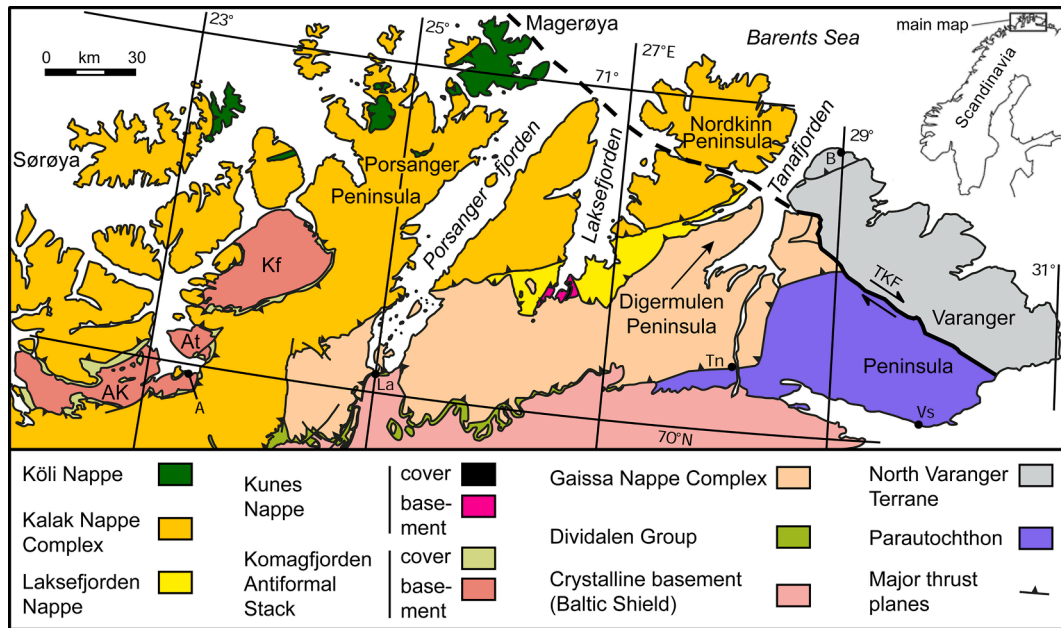
Fig. 1. Simplified geological map of Finnmark, northern Norway (modified after Rice, 2014). The Gaissa Nappe Complex (Lower Allochthon) largely comprises the Tanafjorden, Vestertana and Digermulen groups. The inset (upper right) indicates the location of the map within Scandinavia. Abbreviations of places: A – Alta, B – Berlevåg, La – Lakselv, Tn – Tana Bru, Vs – Vadsø. Abbreviations of geological structures: AK, At, Kf – Alta-Kvænangen, Altenes and Komagfjorden tectonic windows. TKF – Trollfjorden–Komagelva Fault Zone. The study area is on the Digermulen Peninsula at the western side of Tanafjorden.
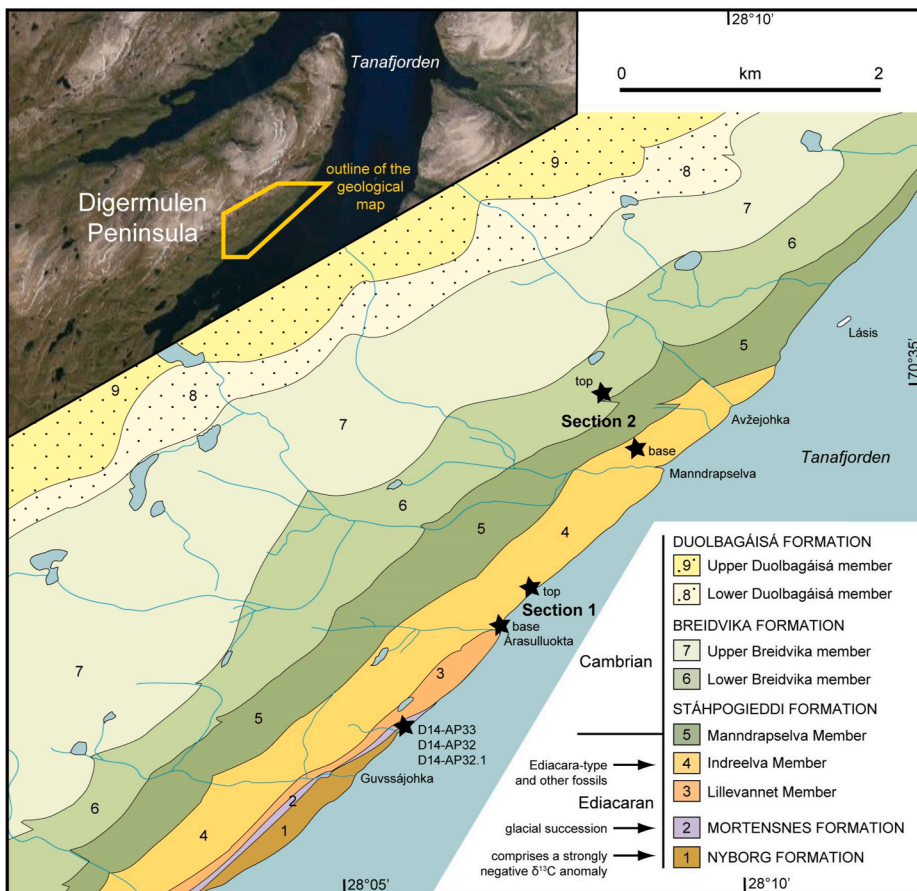
Fig. 2. Geology of the southeast portion of the Digermulen Peninsula, based on Siedlecka et al. (2006), showing localities of the two sections where samples were taken for analyses discussed in this study. The inset (upper left) indicates the location of the geological map on the Digermulen Peninsula. Section 1 comprises the older part of the succession, including the uppermost part of the Nyborg Formation, Mortensnes Formation, and the lower part of the Indreelva Member. No mudstone samples were taken from the Lillevannet Member due to its coarse lithology. The geographic coordinates of the base and top of Section 1 are as follows: N 70°33′51″ and E 028°06′17″ for the base, and N 70°34′18″ and E 028°07′47″ for the top. Section 2 comprises the uppermost part of the Indreelva Member, Manndrapselva Member, and the lower part of the Lower Breidvika member. The geographic coordinates of the base and top of Section 2 are as follows: N 70°34′43″ and E 028°08′60″ for the base, and N 70°34′58″ and E 028°08′31″ for the top.
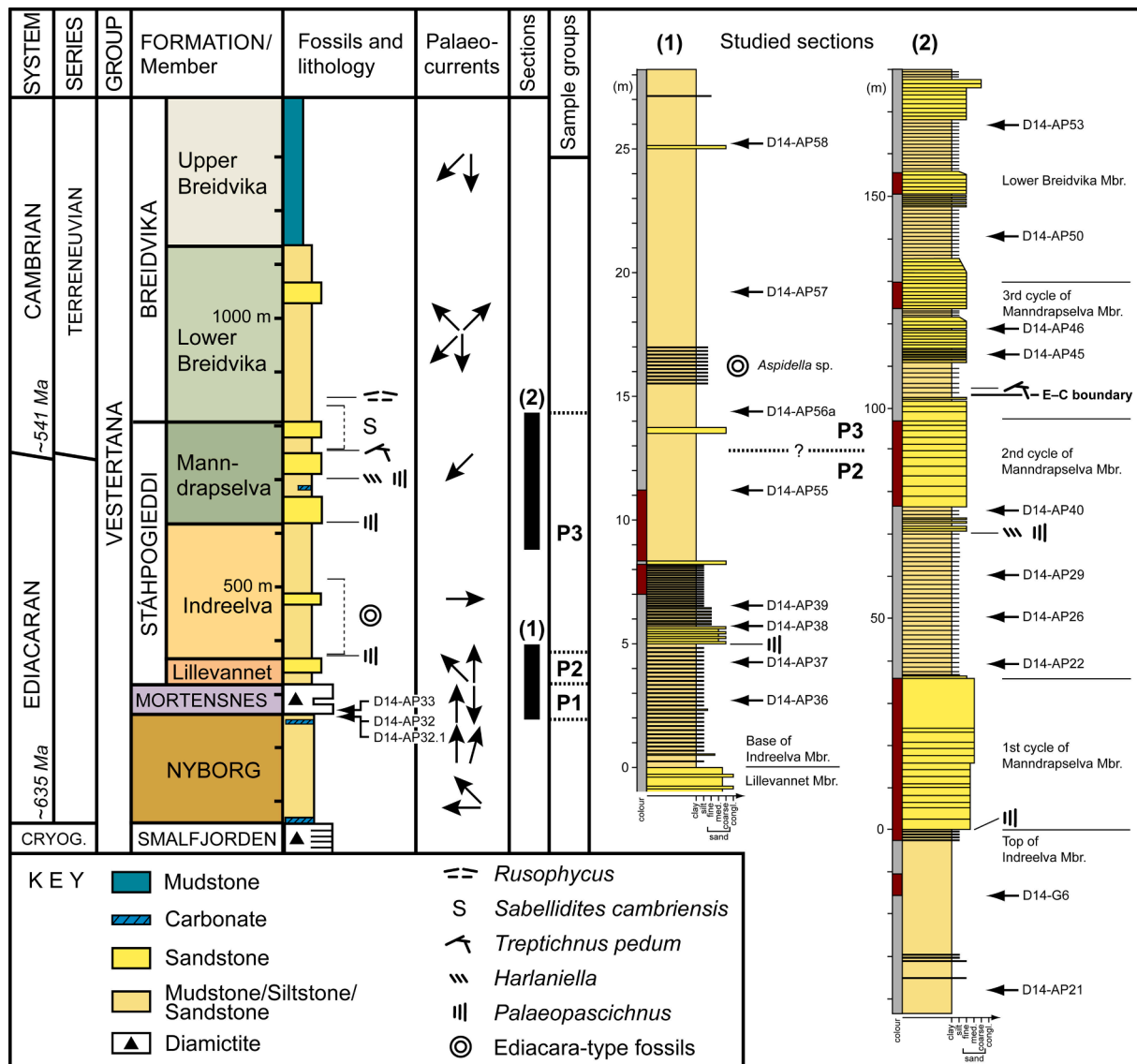
Fig. 3. Simplified stratigraphy of the Vestertana Group (after Jensen et al., 2018b). The distribution of *Sabellidites cambriensis* is according to Ebbestad et al. (2022). Palaeocurrent data were taken from the published literature (Reading, 1965; Banks et al., 1971; Banks, 1973). As an exemplary explanation, an arrow pointing to the top indicates a palaeocurrent flow direction from south to north. On the right side, the stratigraphic range and lithological logs of the two sections analysed in this study are shown with stratigraphic positions of mudstone samples taken for chemical and isotopic analyses being indicated. Stratigraphic heights in Sections 1 and 2 are given with reference to the top of the Lillevannet Member and the Indreelva Member, respectively. The grey and red-brown colours next to the stratigraphic heights indicate the approximate colours of the rock strata. The stratigraphic position of the boundary between the sample groups P2 and P3 is somewhere between samples D14-AP56 and D14-AP56a. The stratigraphic positions of the two mudstone samples from the Nyborg Formation (D14-AP32 and D14-AP32.1) and the single sample from the Mortensnes Formation (D14-AP33) are indicated in the simplified stratigraphic column on the left side.

Jämtland can be extrapolated across a distance of ca. 1000 km to northern Norway peninsulas (e.g., Digermulen and Varanger) is lacking, the suggestion of Kumpulainen et al. (2021) is still equivocal. Furthermore, the arguments discussed by Jensen et al. (2018b) and Agić et al. (2022) support a post-Marinoan age for the Mortensnes Formation.

The postglacial Stáhpogieddi Formation is divided into the Lillevannet, Indreelva and Manndrapselva members (Fig. 3). The lower part of the formation represents a transgressive sequence from the fluvial conditions of the upper part of the Lillevannet Member into the quiet marine conditions of the Indreelva Member (Banks et al., 1971; Banks, 1973), with deposition in a marine environment continuing into the Breidvika Formation (Reading, 1965; Banks et al., 1971). The Stáhpogieddi and Breidvika formations mainly comprise siliciclastic sedimentary rocks (mudstones, siltstones, and sandstones). Recently, Meinhold et al. (2019a) described carbonate beds, lenses and

concretions from the 2nd cycle of the Manndrapselva Member. In a simplified view, palaeocurrent flow directions are mainly to the northwest and north in the older strata (Nyborg and Mortensnes formations and Lillevannet Member), to the east in the Indreelva Member, and to the southwest in the younger strata, with the informal Lower Breidvika member showing bimodal directions (Fig. 3).

On the Digermulen Peninsula, Ediacara-type fossils occur in the Indreelva Member (Farmer et al., 1992; Högström et al., 2013; McIlroy and Brasier, 2017; Jensen et al., 2018a,b) (Fig. 3). *Aspidella*-type discoidal fossils first appear close to the base of the Indreelva Member (Figs. 3, 4a), within a facies dominated by red and green siltstones. A more diverse association of Ediacara-type fossils are found higher in the Indreelva Member in a facies with a higher proportion of sandstone beds. This includes frondose forms (Fig. 4b) and a dickinsoniomorph. In addition, flask-shaped microfossils have recently been described from
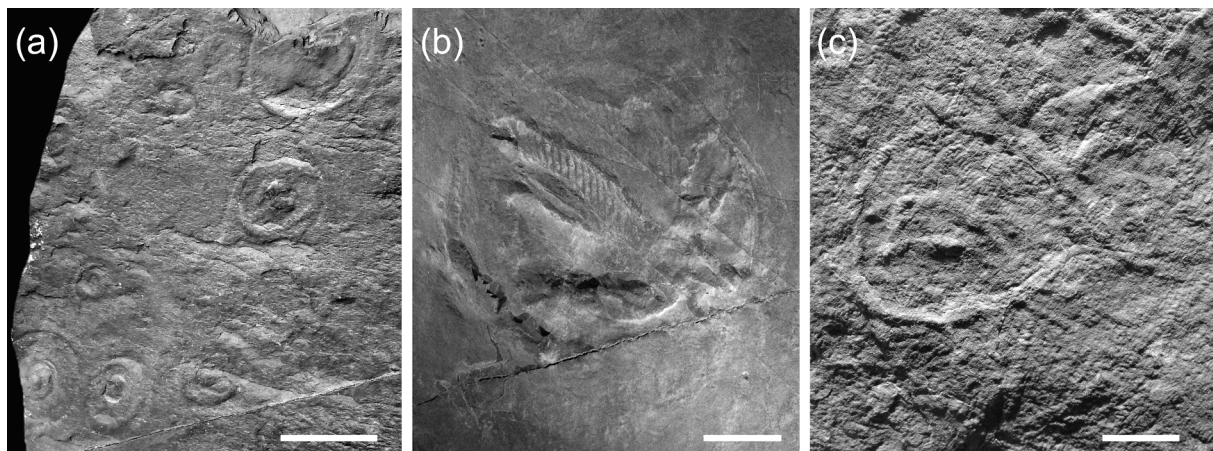
Fig. 4. Examples of late Ediacaran fossils from the Digermulen Peninsula, Arctic Norway. **(a)** *Aspidella*-type discoidal fossils from the basal part of the Indreelva Member in a coastal outcrop north of Árasulluokta. See section 1 in Fig. 3 for stratigraphic level. Scale bar is 50 mm **(b)** Multi-vaned frondose fossil (cf. *Swartpuntia*) from the approximate mid-portion of the Indreelva Member in a coastal outcrop north of Manndrapselva. Scale bar is 20 mm. **(c)**. The non-metazoan fossils *Palaeopascichnus* and *Harlaniella* from the 2nd cycle of the Manndrapselva Member. See section 2 in Fig. 3 for stratigraphic level. Scale bar is 10 mm.

the lower part of the Indreelva Member (Agić et al., 2022). Age constraint for the basal part of the Indreelva Member comes from palaeopascichnids – non-metazoan macroscopic fossils – with expanding segments, which have a global first appearance approximately at 560 Ma (Jensen et al., 2018b; Kolesnikov and Desiatkin, 2022). Based on trace fossils, palaeopascichnids (Fig. 4c), tubular non-mineralized metazoan (*Sabellidites*), and organic-walled microfossils, the Ediacaran–Cambrian boundary is close to the base of the 3rd cycle of the Manndrapselva Member (Högström et al., 2013; McIlroy and Brasier, 2017; Jensen et al., 2018a,b; Agić et al., 2022; Ebbestad et al., 2022) (Fig. 3). The post-depositional low-grade metamorphic overprint of the sedimentary succession of the Digermulen Peninsula is related to a Scandian tectono-metamorphic event at 450–430 Ma (Meinhold et al., 2019b, 2020).

2.2. Detrital zircon U–Pb data

For the later discussion of the sediment provenance based on isotopic data (Section 5.3.) it is essential to summarize some of the published data about detrital zircon U–Pb ages from the Ediacaran and Cambrian sandstones of Finnmark. Detrital zircon U–Pb ages from a sandstone sample of the interglacial Nyborg Formation from the adjacent Varanger Peninsula are mainly 2.0–1.85 Ga, with a minor spread between 3.0 and 2.5 Ga (Roberts and Siedlecka, 2012). No Mesoproterozoic zircon grains were detected. The omnipresence of mid-Palaeoproterozoic zircon grains in the Nyborg Formation points toward a sediment source from the Svecofennian province, with only a minor influx from the Karelian province.

Detrital zircon U–Pb ages from a Manndrapselva Member sandstone sample collected on the mainland of northern Finnmark, just south of the Digermulen Peninsula, yielded one major age peak at 554 Ma, a broad spread of ages between 1620 and 930 Ma, and a subordinate age peak at 645 Ma (Zhang et al., 2015). Also, lower Cambrian sandstones from the Dividalen Group close to the international border between Finland and Norway contain detrital zircon grains with Ediacaran ages besides a broad spread of ages between ca. 2000 and 1000 Ma and a few late Archaean grains (Andresen et al., 2014). Overall, the detrital zircon age spectra from sandstones of the Manndrapselva Member and the Dividalen Group are evidence for mixed sediment influx from old upper crustal sources from the Svecofennian province and juvenile detrital material (ca. 570–550 Ma); the latter is interpreted to be derived from magmatic rocks of the Timanides (Andresen et al., 2014; Zhang et al., 2015). This orogen formed during the late Ediacaran along the north-eastern periphery of Baltica (present-day coordinates) due to accretion of island-arc complexes onto Baltica (Pease et al., 2004).

3. Material and methods

This study is based on fine-grained siliciclastic sedimentary rock samples from surface outcrops along two stratigraphic sections at the eastern side of the Digermulen Peninsula (Figs. 2, 3). In order to understand sediment composition, provenance and post-depositional alteration a total of 21 samples were processed for bulk mineralogy, REE chemistry, and $^{147}Sm–^{143}Nd$ and $^{87}Rb–^{87}Sr$ isotopic analyses. Stratigraphic levels of the samples are shown in Fig. 3. Most of the mudstones are greenish-grey, a few are bluish-grey in colour. Sample D14-G6 is the only sample of brownish-grey colour. We chose fine-grained siliciclastic sedimentary rocks because they normally best reflect the average composition of the source area compared to sandstones or coarser sediments (McCulloch and Wasserburg, 1978; Allègre and Rousseau, 1984; Cullers, 1995). The majority of the samples were also processed for palynological analysis. Initial results (Palacios et al., 2017; Agić et al., 2019, 2022; Teodoro Palacios, unpublished data) as well as biostratigraphic information from macrofossils (Högström et al., 2013; McIlroy and Brasier, 2017; Jensen et al., 2018a,b; Ebbestad et al., 2022) provide constraints on the depositional ages.

The dried sample material was disintegrated with a hammer and thoroughly powdered and homogenized using an agate ball mill. Some of the rock powder was used for X-ray diffraction (XRD) analysis to determine semi-quantitatively the bulk mineralogy of the samples. The analysis was conducted using a Philips X'Pert MPD, equipped with a PW3050 Goniometer. CuKα-radiation, a tube voltage of 40 kV, a tube current of 30 mA, and a scanning range from 4° to 69.5° 2θ was applied. Mineral identification was performed with X'Pert HighScore software package. Semi-quantitative data is based on the RIR method of X'Pert HighScore. XRD analysis was conducted at the Department of Sedimentology and Environmental Geology at the University of Göttingen, Germany.

The remaining rock powder was used for chemical and isotopic analyses. REE were quantified using inductively coupled plasma mass spectrometry (ICPMS) on the dissolved sample material. For each sample, 100 mg of rock powder were digested in the following steps using a PicoTrace® digestion system: (1) pre-reaction with 2 ml HNO_3 at 50 °C overnight, (2) first pressure phase with additional 3 ml HF (40%) and 3 ml $HClO_4$ (70%) at 150 °C for 8 h, (3) evaporation at 180 °C for 16 h, (4) second pressure phase with 10 ml double de-ionised water, 2 ml HNO_3 and 0.5 ml HCl at 150 °C for 4 h. The resulting solution was diluted to 100 ml with ultrapure water. Analysis was performed using a Thermo-Electron VG PlasmaQuad 2 quadrupole ICPMS at the Department of Geochemistry and Isotope Geology at the University of Göttingen.

The REE data were normalized to both CI chondrite and PAAS (Post-Archaean Australian Shale) using the values of Pourmand et al. (2012). Normalisation of trace concentration data removes the natural 'even-odd' variability in the relative cosmological abundances of elements in solar system objects. It thus produces 'smooth' patterns of the samples in trace element plots and allows a more convenient comparison of their patterns.

The calculation of the Ce and Eu anomalies is common practice when dealing with whole-rock geochemical data of fine-grained sedimentary rocks as the Ce anomaly may provide information on redox conditions at the time of deposition (e.g., Wilde et al., 1996; Pattan et al., 2005) and the Eu anomaly on the provenance of the sediment, e.g. composition of the source area (e.g., McLennan, 1989; McLennan et al., 1993; Gao and Wedepohl, 1995). Ce anomalies are increasingly used as a proxy for Earth's oxygenation events and geobiological changes during the Proterozoic and early Phanerozoic (Wallace et al. 2017). Ce anomalies (Ce/Ce*) were calculated following Bau and Dulski (1996): $Ce/Ce^* = Ce_N/(0.5La_N + 0.5Pr_N)$, where the subscript N indicates PAAS-normalized values. To test whether the obtained Ce anomaly values are genuine and not an effect of anomalous La enrichment, we applied the method of Bau and Dulski (1996) and additionally calculated the Pr anomalies (Pr/Pr*) as follows: $Pr/Pr^* = Pr_N/(0.5Ce_N + 0.5Nd_N)$. A negative Ce anomaly inevitably results in $Pr/Pr^* > 1$, whereas a positive Ce anomaly generates $Pr/Pr^* < 1$. The combination of $Ce/Ce^* < 1$ and $Pr/Pr^* < 1$, however, indicates a positive La anomaly and hence non-redox related Ce anomalies (Bau and Dulski, 1996). The Eu anomalies (Eu/Eu*) were calculated as suggested by McLennan (1989): $Eu/Eu^* = Eu_N/(Sm_N \times Gd_N)^{0.5}$, where the subscript N indicates chondrite-normalized values.

Multicollector (MC)-ICPMS analyses of $^{143}Nd/^{144}Nd$ and $^{87}Sr/^{86}Sr$ isotope compositions were performed at the Department of Geochemistry and Isotope Geology at the University of Göttingen. The wet-chemical procedures were performed in class 100 fume hoods housed in a metal-free, class 10,000 clean room environment. Samples were processed with double-distilled HCl, HNO$_3$, and HF prepared by sub-boiling and diluted with high-purity water (18.2 MΩ cm^{-1}) for chromatography. About 50 to 100 mg of sample powder (equivalent to ca. 300 ng Nd and 10 µg of Sr) were weighted into 15 ml screw top PFA beakers and spiked with ^{150}Nd–^{149}Sm and ^{87}Rb–^{84}Sr tracer solutions. Sample powders were digested in a mixture of 2 ml concentrated HNO$_3$ and 2 ml concentrated HF on a hotplate at 120 °C for 72 h and heated at 80 °C to incipient dryness. The sample cake was dissolved in 10 ml of 6 M HCl and heated at 110 °C overnight for complete sample dissolution. When necessary, this step was repeated.

The separation of Sr and Nd from the sample solution generally followed the method described in Hegner et al. (1995, 2010). The cation exchange procedures employed BioRad AG 50 × 8 (200–400 mesh) resin and Triskem Ln-Resin (100–150 µm) to separate Nd and Sm from neighbouring REE. The Sr cut was further purified with Triskem Sr-Resin (50–100 µm; method of Pin et al., 2014) for elimination of any remaining ^{87}Rb interfering with ^{87}Sr during mass spectrometry. The element fractions were diluted in 0.5 M HNO$_3$ to a nominal concentration of samples and reference materials of 100 ng mL^{-1} for mass spectrometry.

The isotope ratios were determined on a ThermoFisher Scientific Neptune Plus MC-ICPMS equipped with nine Faraday cups. The ion currents of Sr and Nd isotopes were measured with 10^{11} Ω amplifiers and the interfering isotope monitors (i.e., ^{140}Ce and ^{149}Sm for Nd isotopes, ^{83}Kr and ^{85}Rb for Sr isotopes, and ^{145}Nd and ^{155}Gd for Sm isotopes) were measured with 10^{12} Ω amplifiers. Sample solutions were introduced into the plasma source via a Teledyne Cetac Aridus3 desolvation system, and the plasma source was equipped with a standard Ni sampler and h-type skimmer cones. $^{143}Nd/^{144}Nd$ and $^{87}Sr/^{86}Sr$ isotope ratio determinations are based on 100 mass scans obtained in static ion-collection mode. Measurements of blank solutions (0.5 M HNO$_3$; 40 scans) preceded and followed those of sample solutions and references materials.

Data reduction was performed off-line using a Python script

employing the 'double' isotope dilution equation of Boelrijk (1968). The average value of the two blank solution analyses was used for correction of acid and gas blank contributions and electronic background. For Sr isotope analyses, the blank- and ^{87}Rb-corrected Sr isotope ratios were normalized to $^{86}Sr/^{88}Sr = 0.1194$ whereas for Nd isotope analyses, the blank- and ^{144}Sm, ^{150}Sm-corrected Nd isotope ratio were normalized to $^{146}Nd/^{144}Nd = 0.7219$ (DePaolo, 1981) using an exponential mass fractionation law. Concentrations of Rb and Sm were determined using an ID-SF-ICPMS technique as described in Willbold and Jochum (2005).

The data are reported relative to $^{87}Sr/^{86}Sr = 0.710247 \pm 10$ (2SD, N = 15) in NIST SRM 987 and $^{143}Nd/^{144}Nd = 0.512093 \pm 7$ (2SD, N = 21) in JNdi-1, which were obtained over a time period of six months. For quality control, the basaltic GSJ reference material JB-2 was analysed and yielded $^{87}Sr/^{86}Sr = 0.703662 \pm 4$ (2SD$_{mean}$), and $^{143}Nd/^{144}Nd = 0.513093 \pm 4$ (2SD$_{mean}$). Isotopic ratios determined in this study are in excellent agreement with the preferred values for JB-2 compiled in the GeoReM database at time of publication ($^{87}Sr/^{86}Sr = 0.703661 \pm 32$ and $^{143}Nd/^{144}Nd = 0.513093 \pm 11$ respectively; https://georem.mpch-mainz.gwdg.de).

$^{143}Nd/^{144}Nd$ ratios are also expressed here in epsilon (ε) notation, i. e. ε$_{Nd}$(0) and ε$_{Nd}$(T), a measure of the difference in $^{143}Nd/^{144}Nd$ from the 'chondritic uniform reservoir' (CHUR), and were calculated using the present-day CHUR values ($^{143}Nd/^{144}Nd = 0.512630$; $^{147}Sm/^{144}Nd = 0.1960$) of Bouvier et al. (2008). For a rock of age T, ε$_{Nd}$(T) is the initial value of ε$_{Nd}$, i.e. the value at the time of formation of the rock, whereas ε$_{Nd}$(0) is the measured value. Although the depositional ages of the Ediacaran mudstone samples have some uncertainty, this does not change the geological interpretation of the data appreciably.

The $^{147}Sm/^{144}Nd$ isotopic ratio is expressed as an enrichment factor ($f_{Sm/Nd}$) relative to CHUR and was calculated following DePaolo and Wasserburg (1967): $f_{Sm/Nd} = ((^{147}Sm/^{144}Nd)_{sample}/(^{147}Sm/^{144}Nd)_{CHUR}) - 1$. It varies inversely with enrichment of LREE, so it is a sensitive indicator of the REE pattern. The Sm–Nd depleted mantle (DM) crustal residence ages (T_{DM}) were calculated using the DM evolution model of Nägler and Kramers (1998) and a decay constant ($\lambda^{147}Sm$) of 6.54 × 10^{-12} year^{-1} (Lugmair and Marti, 1978). The international chronostratigraphic chart (Cohen et al., 2021) was used as a stratigraphic reference for data interpretation.

4. Results

Based on the analytical data (Tables 1–3), significant variations are observed among the studied samples which define three distinct populations referred to as P1, P2, and P3 in the following. P1 includes samples from the Nyborg and Mortensnes formations. P2 includes the lowermost five samples from the Indreelva Member. All the remaining samples are assigned to P3, extending from approximately 2 m below the stratigraphically lowest occurrence of discoidal Ediacara-type fossils in the Indreelva Member (see Section 1 in Fig. 3), including the Manndrapselva Member and up to the Lower Breidvika member (see Section 2 in Fig. 3). In the following, these three populations will be used when describing and discussing the data.

4.1. Mineralogical analysis

Semi-quantitative bulk mineralogy based on XRD is presented in Table 1 and Fig. 5. High amounts of phyllosilicates, mainly illite plus minor amounts of chlorite and biotite, as well as medium amounts of quartz and feldspar are the most prominent minerals in the studied samples. Note that in this study illite data includes muscovite because both 2:1 layer phyllosilicates are difficult to distinguish by semi-quantitative XRD analysis on rock powder. Chlorite can vary from Fe-rich chlorite, known as chamosite, to Mg-rich chlorite, known as clinochlore. Regardless of which phyllosilicate minerals of the chlorite group are present in the samples, they are classified here as chlorite. P1 samples exhibit the highest quartz + feldspar abundances among all

Table 1
Semi-quantitative powder X-ray diffraction (XRD) bulk mineralogy of mudstones analysed in this study. P* refers to the sample populations identified based on provenance characteristics. The stratigraphic position of the samples is shown in Fig. 3. Illite includes illite + muscovite.

P*	Sample	Formation	Member	illite	chlorite	biotite	kaolinite	quartz	feldspar	carbonate	others
	Section 2										
3	D14-AP-53	Breidvika	Lower Member	49	7	4	6	19	15	0	0
3	D14-AP-50	Breidvika	Lower Member	55	3	3	5	19	15	0	0
3	D14-AP-46	Stáhpogieddi	Manndrapselva (3rd cycle)	49	7	5	7	15	16	0	1
3	D14-AP-45	Stáhpogieddi	Manndrapselva (3rd cycle)	56	2	3	4	22	13	0	0
3	D14-AP-40	Stáhpogieddi	Manndrapselva (2nd cycle)	52	5	5	5	20	13	0	0
3	D14-AP-29	Stáhpogieddi	Manndrapselva (2nd cycle)	62	4	0	4	26	4	0	0
3	D14-AP-26	Stáhpogieddi	Manndrapselva (2nd cycle)	68	6	0	0	21	5	0	0
3	D14-AP-22	Stáhpogieddi	Manndrapselva	50	5	4	6	18	17	0	0
3	D14-G6	Stáhpogieddi	Indreelva	57	3	4	0	21	11	0	4
3	D14-AP-21	Stáhpogieddi	Indreelva	49	12	4	0	18	16	0	1
	Section 1										
3	D14-AP-58	Stáhpogieddi	Indreelva	50	8	4	7	11	15	0	5
3	D14-AP-57	Stáhpogieddi	Indreelva	52	6	5	5	21	11	0	0
3	D14-AP-56a	Stáhpogieddi	Indreelva	47	3	4	5	17	13	0	11
2	D14-AP-55	Stáhpogieddi	Indreelva	53	3	2	4	14	21	0	3
2	D14-AP-39	Stáhpogieddi	Indreelva	49	10	4	8	12	17	0	0
2	D14-AP-38	Stáhpogieddi	Indreelva	71	7	0	0	14	8	0	0
2	D14-AP-37	Stáhpogieddi	Indreelva	53	9	4	9	13	12	0	0
2	D14-AP-36	Stáhpogieddi	Indreelva	45	11	4	11	12	17	0	0
1	D14-AP-33	Mortensnes		45	2	3	4	22	21	3	0
1	D14-AP-32	Nyborg		44	4	3	4	14	31	0	0
1	D14-AP-32.1	Nyborg		46	5	4	5	14	25	0	1

samples. The single sample from the Mortensnes Formation contains 3% carbonate (dolomite).

4.2. Rare earth element (REE) data

REE abundances are presented in Table 2. The overall REE patterns of P1 samples are similar but the single sample from the Mortensnes Formation shows an overall depletion in REE (Fig. 6a, b). The chondrite-normalized patterns of the P1 mudstones exhibit enrichment of the LREE (La_N/Sm_N: 3.72 to 4.40, with an average value of 4.12; Table 2), relatively flat patterns for the heavy REE (HREE include Eu, Gd, Tb, Dy, Ho, Er, Tm, Yb, and Lu), with Gd_N/Yb_N values showing some variation (1.49 to 1.61, with an average value of 1.56). The single sample from the Mortensnes Formation has the lowest La_N/Yb_N (8.77) compared with La_N/Yb_N from the other samples of P1 (10.39 and 11.84). The Ce and Eu anomalies range from 0.98 to 1.00 (0.99 on average) and 0.52 to 0.63 (0.56 on average), respectively (Fig. 7a). The PAAS-normalized REE patterns are relatively flat with Nyborg Formation mudstones having higher REE abundances than PAAS while the single sample from the Mortensnes Formation has lower REE abundances than PAAS (Fig. 6b).

The chondrite-normalized patterns of P2 mudstones exhibit enrichment of the LREE (La_N/Sm_N: 4.73 to 5.23, with an average value of 4.91; Table 2), a depletion of the HREE, with Gd_N/Yb_N values showing prominent variation (0.94 to 2.78, with an average value of 2.11) (Fig. 6c, d). La_N/Yb_N of P2 shows overall the highest values among all the studied samples (15.30 to 22.49, with an average value of 19.65; Table 2). The Ce anomalies range from 0.82 to 0.88 (0.85 on average) and hence are lower than those of P1 (Fig. 7a). On the contrary, the Eu anomalies range from 0.64 to 0.85 (0.76 on average) and hence are higher than those of P1. Sample D14-AP-38 shows a pronounced negative Gd anomaly in both the chondrite- and PAAS-normalized REE patterns (Fig. 6c, d). All P2 mudstones exhibit depletion of the HREE with respect to PAAS (Fig. 6d).

The overall REE patterns of P3 mudstones are similar (Fig. 6e–h). For illustration purposes, however, P3 has been split into two subsets. The remaining samples of the Indreelva Member are shown in Fig. 6e, f and those from the Manndrapselva Member and the Lower Breidvika member are shown in Fig. 6g, h. The chondrite-normalized patterns of the P3 mudstones exhibit enrichment of the LREE (La_N/Sm_N: 3.10 to 6.68, with an average value of 4.74; Table 2), relatively flat patterns for the HREE, with Gd_N/Yb_N values showing some variation (0.78 to 1.76,

with an average value of 1.39). La_N/Yb_N ranges from 7.45 to 15.73 (10.07 on average). The Ce and Eu anomalies range from 0.96 to 1.01 (0.98 on average) and 0.50 to 0.87 (0.65 on average), respectively. The PAAS-normalized REE patterns are relatively flat (Fig. 6f, h). Sample D14-AP-29 shows a pronounced negative Gd anomaly in both the chondrite- and PAAS-normalized REE patterns (Fig. 6g, h).

Fig. 7b shows Gd_N/Yb_N plotted against La_N/Sm_N. Many samples plot near PAAS, one sample of P2 and four samples of P3 show La_N/Sm_N (>5.0), and four samples of P2 show high Gd_N/Yb_N (>2.0).

4.3. ^{147}Sm–^{143}Nd isotopic data

Sm–Nd isotopic data are presented in Table 3 and illustrated in Figs. 8, 9. Significant variations are observed among the three populations. P1 has $^{143}Nd/^{144}Nd$ initial ratios ranging from 0.511250 to 0.511305 (with an average value of 0.511285), $\varepsilon_{Nd}(0)$ values ranging from −18.09 to −18.65, $\varepsilon_{Nd}(T)$ values ranging from −11.08 to −12.40, and ^{147}Sm–^{143}Nd depleted mantle (DM) crustal residence ages (T_{DM}) of 1830 to 2045 Ma. P2 samples have a significantly different isotopic composition. They have $^{143}Nd/^{144}Nd$ initial ratios ranging from 0.510834 to 0.510868 (with an average value of 0.510850), the most negative $\varepsilon_{Nd}(0)$ values, ranging from −25.64 to −28.30, $\varepsilon_{Nd}(T)$ values ranging from −20.37 to −21.04, and the oldest T_{DM} ages, ranging from 2360 to 2840 Ma. P3 has $^{143}Nd/^{144}Nd$ initial ratios ranging from 0.511804 to 0.511991 (with an average value of 0.511902), $\varepsilon_{Nd}(0)$ values ranging from −12.46 to −16.11, $\varepsilon_{Nd}(T)$ values ranging from −6.00 to −9.01, and T_{DM} ages of 1405 to 1960 Ma.

Fig. 8a illustrates the separation of the stratigraphic succession into three units based on the Sm–Nd isotopic signatures. Fig. 8b combines REE abundances and Nd isotopic composition, with $f_{Sm/Nd}$ being an expression of the slope of the REE pattern between Nd and Sm (McLennan and Hemming, 1992; Bock et al., 1994; Lev et al., 1999). A chondritic mantle has an $f_{Sm/Nd}$ of 0.0, LREE-depleted mantle has an $f_{Sm/Nd}$ of about +0.1 and a typical LREE-enriched upper crustal rock has an $f_{Sm/Nd}$ of about −0.4 (Taylor and McLennan, 1985). For all samples, regardless of which population they belong, $f_{Sm/Nd}$ values range between −0.330 and −0.576 (−0.476 on average) (Fig. 8b).

4.4. ^{87}Rb–^{87}Sr isotopic data

^{87}Rb–^{87}Sr isotopic data are presented in Table 3. With the exception

Table 2

Rare earth element (REE) abundances in parts per million (ppm) of mudstones analysed in this study. P* refers to the sample populations identified based on provenance characteristics. The stratigraphic position of the samples is shown in Fig. 3. Sm and Nd values were obtained by isotope dilution thermal ionization mass spectrometry (ID-TIMS). All other REE data were obtained by ICP-MS.

P*	Sample	Formation	Member	La	Ce	Pr	Nd	Sm	Eu	Gd	Tb	Dy	Ho	Er	Tm	Yb	Lu	La$_N$/Yb$_N$	La$_N$/Sm$_N$	Gd$_N$/Yb$_N$
Section 2																				
3	D14-AP-53	Breidvika	Lower Member	50.91	103.17	12.45	42.7	5.98	1.30	6.05	0.90	5.75	1.19	3.49	0.50	3.51	0.51	9.97	5.37	1.40
3	D14-AP-50	Breidvika	Lower Member	55.91	111.52	13.27	42.9	6.16	1.30	5.96	0.90	6.03	1.29	3.88	0.57	3.98	0.57	9.64	5.72	1.21
3	D14-AP-46	Stáhpogieddi	Manndrapselva	63.37	126.94	15.53	51.8	7.45	1.55	7.53	1.13	7.31	1.52	4.43	0.63	4.35	0.62	9.99	5.36	1.40
3	D14-AP-45	Stáhpogieddi	Manndrapselva	35.56	73.64	9.38	33.3	7.24	1.62	7.12	1.03	6.04	1.19	3.36	0.48	3.27	0.47	7.45	3.10	1.76
3	D14-AP-40	Stáhpogieddi	Manndrapselva	60.29	120.50	14.74	52.6	8.10	1.39	6.83	1.00	6.43	1.35	4.01	0.58	4.12	0.59	10.05	4.69	1.34
3	D14-AP-29	Stáhpogieddi	Manndrapselva	47.80	97.94	12.73	35.7	5.74	1.25	3.29	0.81	5.33	1.11	3.26	0.49	3.40	0.49	9.64	5.25	0.78
3	D14-AP-26	Stáhpogieddi	Manndrapselva	60.62	125.59	15.97	43.4	8.32	1.96	7.06	1.40	8.94	1.79	4.95	0.70	4.60	0.64	9.04	4.59	1.24
3	D14-AP-22	Stáhpogieddi	Manndrapselva	41.90	83.31	10.25	34.9	6.66	1.39	5.96	0.86	5.18	1.07	3.08	0.45	3.12	0.44	9.21	3.96	1.54
3	D14-G6	Stáhpogieddi	Indreelva	35.95	72.69	8.64	31.0	5.40	1.06	4.61	0.68	4.31	0.90	2.70	0.40	2.85	0.42	8.66	4.20	1.31
3	D14-AP-21	Stáhpogieddi	Indreelva	37.35	72.89	8.91	31.4	5.73	1.21	5.15	0.75	4.41	0.91	2.65	0.38	2.70	0.38	9.50	4.11	1.54
Section 1																				
3	D14-AP-58	Stáhpogieddi	Indreelva	42.60	83.83	9.98	35.3	6.54	1.22	5.39	0.71	4.29	0.91	2.72	0.38	2.74	0.40	10.68	4.11	1.59
3	D14-AP-57	Stáhpogieddi	Indreelva	38.69	77.56	8.91	31.5	5.40	0.95	4.20	0.54	3.34	0.71	2.2	0.32	2.33	0.34	11.41	4.52	1.46
3	D14-AP-56a	Stáhpogieddi	Indreelva	51.65	97.32	11.24	35.4	4.87	0.73	4.02	0.50	3.16	0.67	2.13	0.31	2.25	0.33	15.73	6.68	1.44
3	D14-AP-55	Stáhpogieddi	Indreelva	38.01	60.88	8.12	24.0	4.85	1.16	4.39	0.59	3.29	0.63	1.76	0.24	1.70	0.24	15.3	4.94	2.09
2	D14-AP-39	Stáhpogieddi	Indreelva	51.71	85.15	11.69	41.6	6.63	1.46	5.08	0.62	3.42	0.65	1.85	0.24	1.66	0.23	21.32	4.91	2.47
2	D14-AP-38	Stáhpogieddi	Indreelva	55.59	96.11	14.39	42.9	6.70	1.03	1.96	0.52	3.09	0.58	1.63	0.24	1.70	0.24	22.49	5.23	0.94
2	D14-AP-37	Stáhpogieddi	Indreelva	54.59	92.93	12.20	42.8	7.27	1.69	6.13	0.77	4.09	0.75	2.00	0.26	1.78	0.24	20.98	4.73	2.78
2	D14-AP-36	Stáhpogieddi	Indreelva	48.00	83.15	10.75	38.4	6.39	1.22	5.13	0.67	3.74	0.72	2.04	0.27	1.81	0.26	18.15	4.73	2.29
1	D14-AP-33	Mortensnes		27.42	56.04	6.65	25.2	4.65	0.93	4.27	0.61	3.74	0.77	2.25	0.31	2.15	0.30	8.77	3.72	1.61
1	D14-AP-32	Nyborg		54.31	108.08	12.66	46.5	8.05	1.28	6.60	0.90	5.59	1.18	3.62	0.51	3.58	0.51	10.39	4.25	1.49
1	D14-AP-32.1	Nyborg		63.60	125.05	14.82	55.0	9.12	1.41	7.15	0.93	5.75	1.20	3.79	0.53	3.68	0.53	11.84	4.40	1.57

of the single sample from the Mortensnes Formation, the trace element abundances of Rb and Sr of the mudstones from all three populations show no significant differences. Rb and Sr abundances range from 93 to 220 ppm (with an average value of 158 ppm) and 14 to 132 ppm (with an average value of 53 ppm), respectively. Rb/Sr ratios range from 0.7 to 10.2 (with an average value of 4.1). The single sample from the Mortensnes Formation has the lowest Rb and highest Sr concentrations and hence the lowest Rb/Sr ratio. The Rb–Sr isotopic data yield an error-chron age of ca. 430 Ma and an initial $^{87}Sr/^{87}Sr$ composition of 0.7352 (Fig. 10).

5. Discussion

5.1. Mineralogical analysis

Whole-rock XRD analyses reveal that the Ediacaran and Cambrian samples from the Digermulen Peninsula are carbonate-free, with the exception of sample D14-AP-33 from the glaciogenic Mortensnes Formation (belonging to P1) which contains a minor amount of carbonate (dolomite) (Table 1). The carbonate is likely primary since parts of the Mortensnes Formation diamictites comprise clasts and matrix with dolomitic composition (Rice et al., 2011; and own observations). Nonetheless, all data plot on (or close to) the line between the clay and quartz end-members in the ternary diagram for mudstone classification (Fig. 5). All samples have a clay content > 50% and thus are argillaceous mudstones.

5.2. Rare earth element (REE) data

Chondrite- and PAAS-normalized REE patterns of the mudstones reveal differences among the samples (Fig. 6). Several interpretations may be put forward to explain the variation in REE patterns (Bock et al., 1994): (1) physical sorting of mineral phases enriched in REE (Cullers et al., 1975; McLennan, 1989; Cullers, 1995), (2) mixing of upper crustal sources with a component with relatively LREE-depleted patterns, e.g. mantle-derived, volcanic material (McLennan et al., 1990), (3) sedimentary modification of the REE during weathering and/or early diagenesis, and (4) modification of the REE during later diagenesis and/or tectono-metamorphic overprint (Milodowski and Zalasiewicz, 1991; Lev et al., 1999). The first option can play an important role when comparing sediments of different grain sizes, such as mudstones and sandstones and sediments deposited under different depositional environments (e.g., fluvial versus marine). Physical sorting has a greater influence on the chemical signature of sandstone than on mudstone (Cullers, 1995). In this study, sedimentary rocks of similar grain size (mudstone) and of similar depositional environment (marine) were analysed and hence physical sorting of mineral phases can be neglected or may have played only a minor role. The third and fourth options may have played a role but if so, they would have affected all samples and not a selected subset alone. The most likely interpretation to explain the overall variation in the REE patterns (i.e. variations in LREE to HREE abundances) is change in provenance through time, i.e. mixing of upper crustal sources with different REE patterns. This is confirmed by Nd isotopic studies as outlined in Section 5.3.

Compared to all other samples, P2 mudstones show a strong HREE depletion increasing from Gd to Lu (Fig. 6c, d). Zircon is one of the most common accessory minerals in siliciclastic sediments and sedimentary rocks (Pettijohn, 1941) and a main carrier of HREE, showing increasing values from Gd to Lu in normalized REE patterns (Belousova et al., 2002; Rubatto, 2002). Zircon that crystallized under the presence of garnet will show lower HREE concentration than zircon that crystallized under the absence of garnet (Rubatto, 2002; Taylor et al., 2017). Because zircon is stable during weathering and diagenesis (Pettijohn, 1941) post-depositional modification can be excluded and the HREE depletion in P2 mudstones reflects the characteristics of the source area (provenance). The REE depletion observed in the single sample from the Mortensnes

Table 3

Rb–Sr and Sm–Nd whole-rock isotopic data of mudstones analysed in this study. P* refers to the sample populations identified based on provenance characteristics. The stratigraphic position of the samples is shown in Fig. 3. Column 'Depositional age (Ma)' indicates the approximate stratigraphic age used to calculate ε_{Nd}(T) values. Rb and Sr values were obtained by isotope dilution thermal ionization mass spectrometry, Sr using a Neptun multi-collector inductively coupled plasma mass spectrometer and Rb using a ThermoFisher Scientific Element2 single-collector inductively coupled plasma mass spectrometer. The 'external' relative standard deviation (1RSD) of Rb/Sr (using several sessions) is 0.4% (relative), the 1RSE of individual analysis is about 0.2% (relative). Analytical details about the isotope measurements are given in Section 3.

| P*	Sample	Formation	Member	Depositional age (Ma)	Rb (ppm)	Sr (ppm)	^{87}Rb/^{86}Sr	^{87}Sr/^{86}Sr	2 s (m)	Sm (ppm)	Nd (ppm)	^{147}Sm/^{144}Nd	^{143}Nd/^{144}Nd	2 s (m)	$f_{Sm/Nd}$	^{143}Nd/^{144}Nd$_{(i)}$	ε_{Nd}(0)	ε_{Nd}(T)	T_{DM} (Ma)
	Section 2																		
3	D14-AP-53	Breidvika	Lower Member	530	165	42.6	11.203	0.800654	0.000006	5.98	42.7	0.0845	0.511866	0.000002	−0.569	0.511573	−14.90	−7.36	1435
3	D14-AP-50	Breidvika	Lower Member	535	182	43.3	12.158	0.808550	0.000007	6.16	42.9	0.0866	0.511827	0.000003	−0.558	0.511524	−15.66	−8.19	1500
3	D14-AP-46	Stáhpogieddi	Manndrapselva	537	208	43.7	13.776	0.815938	0.000006	7.45	51.8	0.0868	0.511914	0.000002	−0.557	0.511608	−13.98	−6.49	1405
3	D14-AP-45	Stáhpogieddi	Manndrapselva	537	141	47.9	8.505	0.779798	0.000010	7.24	33.3	0.1313	0.511991	0.000003	−0.330	0.511530	−12.46	−8.03	1960
3	D14-AP-40	Stáhpogieddi	Manndrapselva	540	187	58.1	9.310	0.797187	0.000008	8.10	52.6	0.0930	0.511804	0.000002	−0.526	0.511475	−16.11	−9.01	1600
3	D14-AP-29	Stáhpogieddi	Manndrapselva	542	173	43.0	11.674	0.811509	0.000010	5.74	35.7	0.0971	0.511929	0.000006	−0.505	0.511584	−13.68	−6.84	1500
3	D14-AP-26	Stáhpogieddi	Manndrapselva	543	209	37.9	15.948	0.828502	0.000010	8.32	43.4	0.1157	0.511969	0.000005	−0.410	0.511557	−12.89	−7.33	1700
3	D14-AP-22	Stáhpogieddi	Manndrapselva	543	163	24.3	19.434	0.849007	0.000011	6.66	34.9	0.1153	0.511972	0.000004	−0.412	0.511562	−12.83	−7.24	1690
3	D14-G6	Stáhpogieddi	Indreelva	545	145	14.2	29.639	0.912486	0.000008	5.40	31.0	0.1051	0.511853	0.000003	−0.464	0.511478	−15.16	−8.83	1700
3	D14-AP-21	Stáhpogieddi	Indreelva	547	136	19.1	20.526	0.857645	0.000009	5.73	31.4	0.1100	0.511915	0.000003	−0.439	0.511520	−13.96	−7.96	1690
	Section 1																		
3	D14-AP-58	Stáhpogieddi	Indreelva	560	125	23.4	15.481	0.826881	0.000012	6.54	35.3	0.1119	0.511930	0.000003	−0.429	0.511520	−13.65	−7.64	1700
3	D14-AP-57	Stáhpogieddi	Indreelva	560	155	24.1	18.606	0.847540	0.000008	5.40	31.5	0.1034	0.511845	0.000003	−0.473	0.511466	−15.30	−8.69	1685
3	D14-AP-56a	Stáhpogieddi	Indreelva	560	153	46.8	9.476	0.783579	0.000007	4.87	35.4	0.0831	0.511908	0.000003	−0.576	0.511604	−14.08	−6.00	1370
2	D14-AP-55	Stáhpogieddi	Indreelva	560	167	64.3	7.506	0.780174	0.000008	4.85	24.0	0.1221	0.511316	0.000003	−0.377	0.510868	−25.64	−20.37	2840
2	D14-AP-39	Stáhpogieddi	Indreelva	560	144	79.3	5.248	0.767956	0.000007	6.63	41.6	0.0962	0.511190	0.000003	−0.509	0.510837	−28.09	−20.98	2385
2	D14-AP-38	Stáhpogieddi	Indreelva	560	134	95.9	4.059	0.759508	0.000007	6.70	42.9	0.0942	0.511179	0.000003	−0.519	0.510834	−28.30	−21.04	2360
2	D14-AP-37	Stáhpogieddi	Indreelva	560	119	100	3.458	0.754209	0.000007	7.27	42.8	0.1026	0.511241	0.000003	−0.477	0.510865	−27.09	−20.43	2450
2	D14-AP-36	Stáhpogieddi	Indreelva	560	114	84.9	3.876	0.762269	0.000007	6.39	38.4	0.1004	0.511213	0.000003	−0.488	0.510845	−27.65	−20.83	2440
1	D14-AP-33	Mortensnes		580	93	132	2.055	0.743013	0.000006	4.65	25.2	0.1115	0.511674	0.000005	−0.431	0.511250	−18.65	−12.40	2045
1	D14-AP-32	Nyborg		590	193	50.1	11.168	0.812237	0.000008	8.05	46.5	0.1045	0.511703	0.000004	−0.467	0.511299	−18.09	−11.21	1885
1	D14-AP-32.1	Nyborg		590	220	43.4	14.650	0.833264	0.000010	9.12	55.0	0.1000	0.511692	0.000003	−0.490	0.511305	−18.30	−11.08	1830
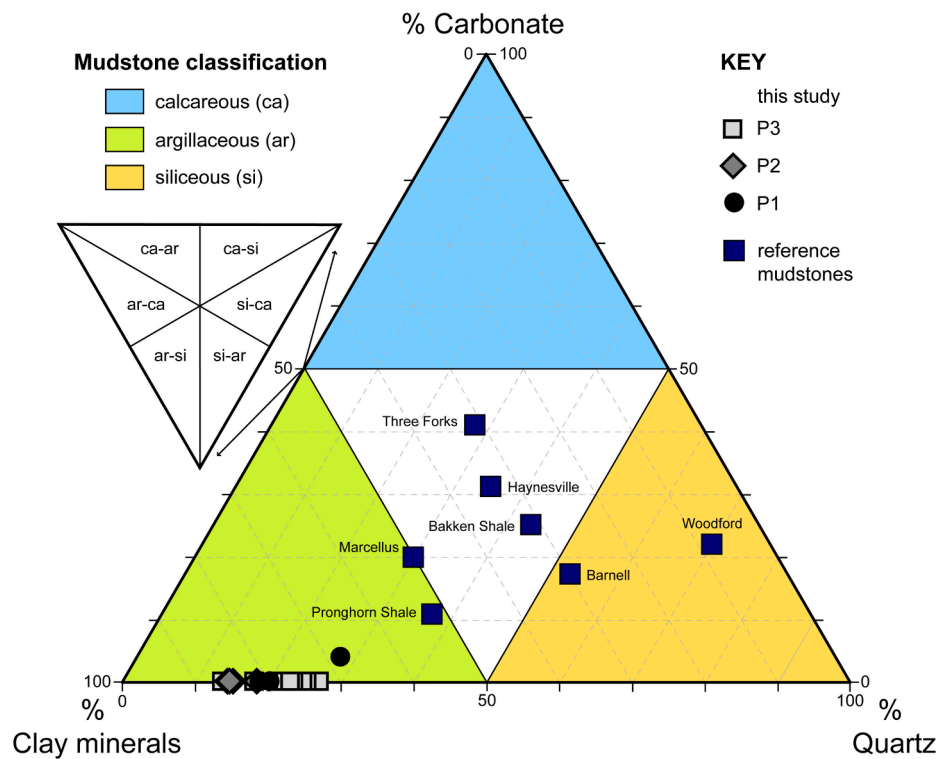
Fig. 5. Classification of mudstone samples (according to the nomenclature of Lazar et al., 2015) analysed in this study based on powder XRD bulk mineralogy (Table 1). Well-known Palaeozoic mudstones from the USA are shown for comparison (blue squares; Anderson, 2014).

Formation is likely a dilution effect due to carbonate enrichment, as this sample has about 3% dolomite (Table 1).

The Ce anomaly in fine-grained sedimentary rocks is commonly used as a fingerprint for the bottom-water redox environment at the time of deposition (e.g., Wilde et al., 1996; Pattan et al., 2005). As Ce has a relatively short mean ocean residence time of only 50–130 years (Alibo and Nozaki, 1999), the Ce anomaly will display a local–regional redox signal (e.g., Shields and Stille, 2001). Changes in bottom-water redox conditions that can influence the Ce anomaly transfer to the sedimentary record may be caused, among others, by sea-level changes (Wilde et al., 1996). Limitations of the application of the Ce anomaly as a palaeoredox proxy may exist in high sedimentation rate areas of continental margin environments (Nath et al., 1997). Increasing dissolved oxygen values in ocean water during the Ediacaran may have provided a first-order control on redox evolution through regulating circulation mechanisms and thus the evolution of the earliest known metazoans (Bowyer et al., 2017). Following the method of Bau and Dulski (1996), P1 mudstones and a few from P3 do not display any Ce anomaly while all P2 mudstones and some from P3 display true negative Ce anomalies (Fig. 7a; Table 2). The true negative Ce anomalies are a clear indication that P2 mudstones and some from P3 were deposited under well-oxygenated seafloor conditions.

The absence of any Ce anomaly in P1 mudstones and few from P3 allows two interpretations. The sediments could have been deposited under anoxic bottom-water conditions. Alternatively, they may have been deposited under oxic bottom-water conditions but in a restricted (near-shore) setting or enclosed bay in a highly evaporitic environment that can preclude Ce anomaly formation (Tostevin et al., 2016a, and references therein). The upper part of the Nyborg Formation was deposited in a tide-influenced setting, indicated by herringbone cross-bedding as well as flaser and lenticular bedding (Banks et al., 1971; and own observations). Such an environment is affected by tidal forcing which can lead to extremely high temporal and spatial shifts in oxygen availability in the water column and porewaters (Taillefert et al., 2007). Consequently, although either depositional environment is permissible,

the cross-stratified beds in P1 combined with the large negative Ce anomalies dominating P2 and P3 seem to favor oxic bottom conditions throughout the succession. The overall change to a shallow water environment in the upper part of the Nyborg Formation may have been associated with the eustatic sea-level fall which occurred with the onset of the Gaskiers glaciation (Banks et al., 1971; and own observations).

The Eu anomaly in fine-grained sedimentary rocks is a good fingerprint for source rock characterization (e.g., McLennan, 1989; McLennan et al., 1993). Positive or no Eu anomalies are often an indication of REE inputs from plagioclase, because this mineral commonly becomes enriched in Eu during crystallization as Eu^{2+} partly substitutes for Ca^{2+} (Taylor and McLennan, 1985; McLennan, 1989; Gao and Wedepohl, 1995). Thus, positive or no Eu anomalies in sediments are considered to reflect influx from juvenile undifferentiated arc rocks, characterizing active continental-margin settings (McLennan, 1989; McLennan et al., 1993; Gao and Wedepohl, 1995). Negative Eu anomalies are commonly associated with felsic minerals that precipitate from late-stage magmas, depleted in Eu. Negative Eu anomalies in sediments are considered to reflect influx from either differentiated arc rocks or old upper continental crust or recycled sedimentary rocks, with the latter two characterizing evolved stable cratons (McLennan, 1989; McLennan et al., 1993; Gao and Wedepohl, 1995). The mudstones studied here display variable, significant negative Eu anomalies (Fig. 6). These values suggest that intracrustal differentiation processes such as partial melting or fractional crystallization had affected the source rocks. Thus, differentiated arc rocks, old upper continental crust and/or recycled sedimentary rocks supplied most of the detrital material. P2 mudstones seem to have received the least differentiated material compared with the other samples.

Two samples, D14-AP-29 and D14-AP-38, show distinct negative Gd anomalies in chondrite- and PAAS-normalized diagrams (Fig. 6c, d, g, h). Also, sample D14-AP-26 shows a negative Gd anomaly but it is less pronounced compared to the other two samples. As the overall dataset and normalized REE patterns appear homogenous, we consider the negative Gd anomalies to be true anomalies and not an analytical
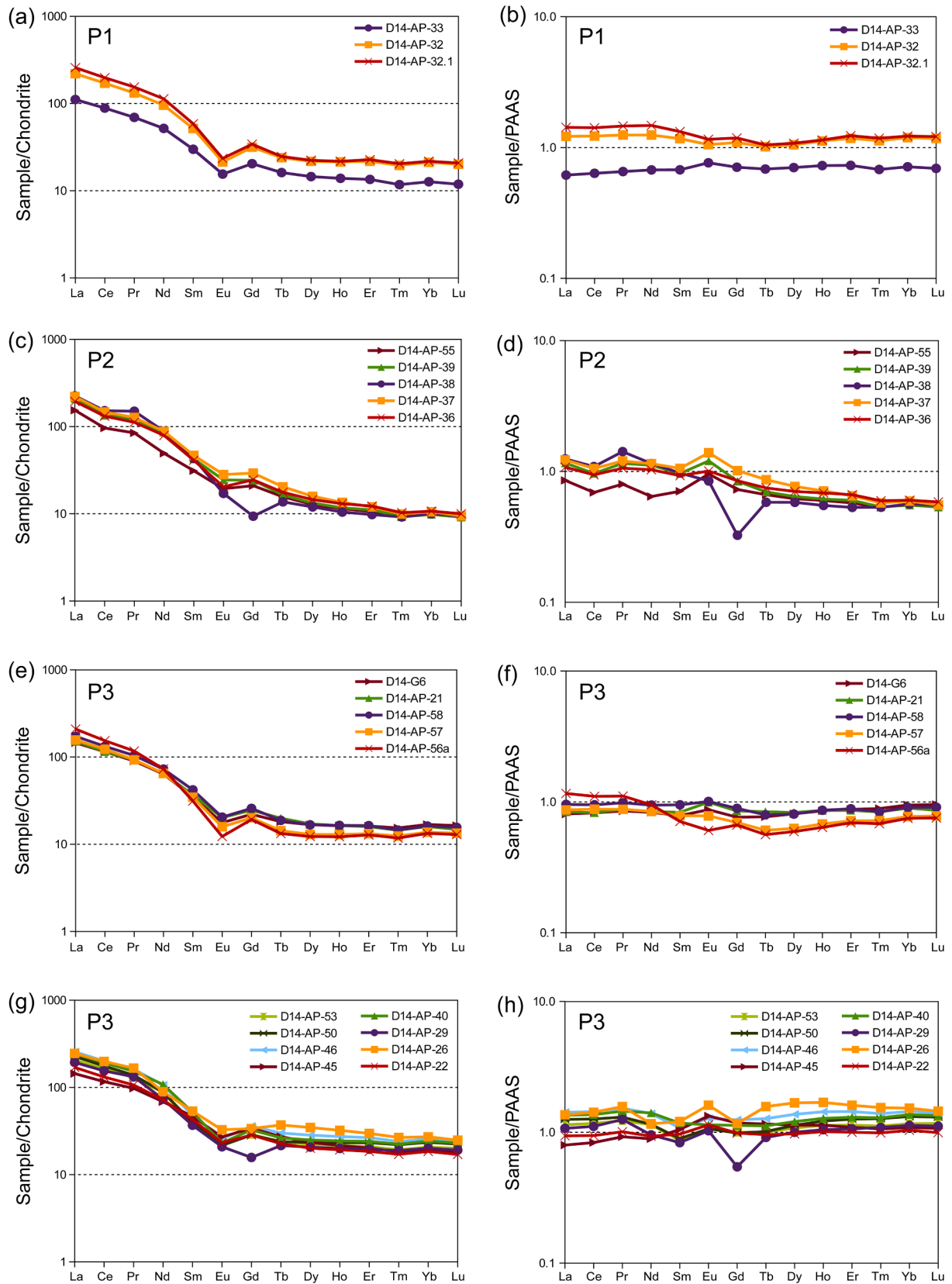
Fig. 6. Normalized REE patterns of mudstones analysed in this study. Normalization was carried out against CI chondrite and Post-Archaean Australian Shale (PAAS) using the revised CI chondrite and PAAS values of Pourmand et al. (2012). **(a–d)** Mudstones from Ediacaran glacial–interglacial cycle. **(e–h)** Mudstones across the Ediacaran–Cambrian boundary.
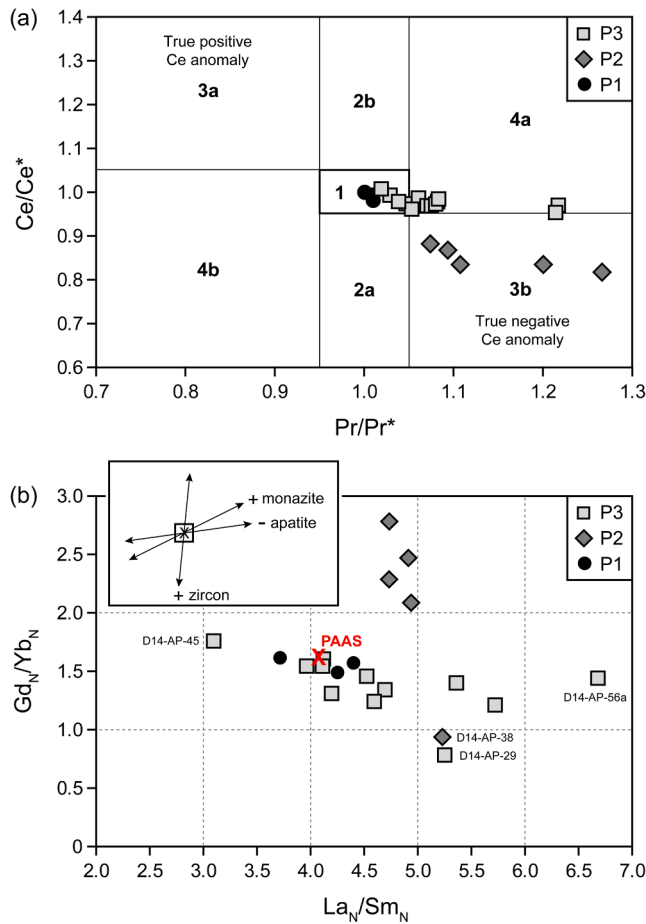
Fig. 7. (**a**) Plot of Pr/Pr* versus Ce/Ce* (after Bau and Dulski, 1996) to reveal genuine Ce anomalies. The distinct fields are defined as follows: 1 – neither Ce nor La anomaly; 2a – positive La, no Ce anomaly; 2b – negative La, no Ce anomaly; 3a – positive Ce and negative La anomaly; 3b – negative Ce and positive La anomaly; 4a – negative Ce and negative La anomaly; 4b – positive Ce and positive La anomaly. (**b**) Plot of La_N/Sm_N versus Gd_N/Yb_N (after Bock et al., 1994). The inset shows the effects of heavy mineral sorting for apatite, monazite, and zircon, with the minus and plus symbols indicating loss and addition, respectively. Normalization was carried out against CI chondrite (Pourmand et al., 2012). Post-Archaean Australian Shale (PAAS, values from Pourmand et al., 2012) shown for reference. Samples around the PAAS composition appear "normal" in regard of their REE composition. Samples away from the PAAS composition suggests that these samples have been influenced by a REE redistributing process.

artefact. Although not very common, negative Gd anomalies in sedimentary rocks have been described in the literature. Bhandari et al. (1996) studied samples from the Cretaceous–Tertiary boundary clay layer at Anjar in the Kutch district of western India. Two of their samples from the boundary interval show negative Gd anomalies in both chondrite- and shale-normalized REE diagrams. Also, mangrove sediment – rich in dissolved organic carbon (Orem et al., 1986; Dittmar et al., 2006) – sometimes shows a negative Gd anomaly (Prasad and Ramanathan, 2008). The Gd anomaly may be controlled by ocean water circulation, biogeochemical cycling of nutrients, and some trace metals (Alibo and Nozaki, 1999). As the reason for the negative Gd anomaly is not clearly understood, it is not further discussed here.

In a La_N/Sm_N versus Gd_N/Yb_N diagram (Fig. 7b), the influence of the enrichment or depletion of specific heavy minerals on the REE abundances in the sediment can be studied (Bock et al., 1994). Many samples plot near PAAS have an average shale composition. Five samples have elevated La_N/Sm_N, likely related to a depletion in apatite. Four samples from the group P2 have $Gd_N/Yb_N > 2.0$; in general, the Gd_N/Yb_N of
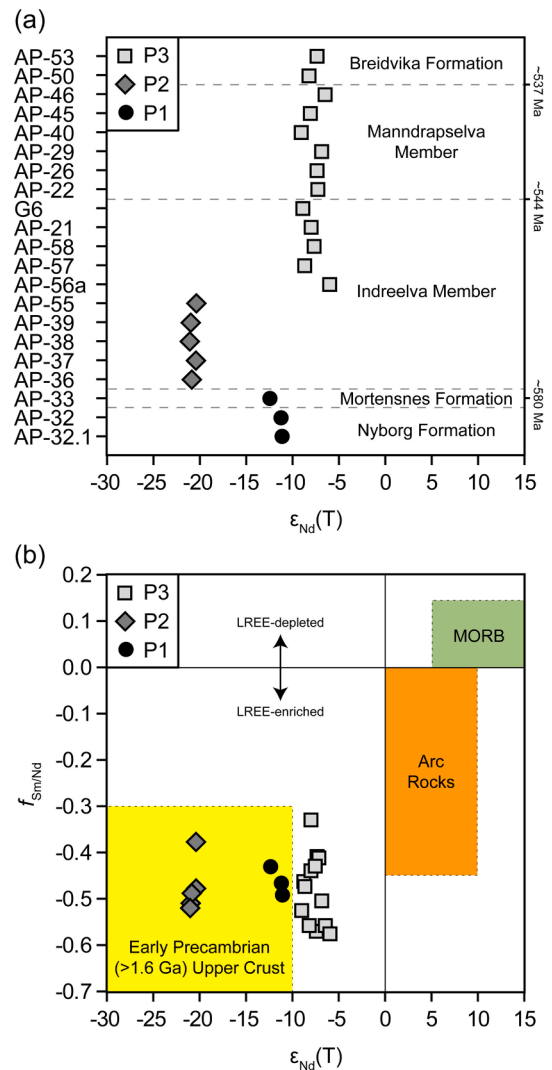
Fig. 8. (**a**) Plot of εNd(T) versus stratigraphic ages of the samples. The samples (without the prefix 'D14-') are arranged from old (base) to young (top). (**b**) Plot of εNd(T) versus $f_{Sm/Nd}$, with reference fields after McLennan and Hemming (1992). Vertical variation of $f_{Sm/Nd}$ can be explained by depletion or enrichment of LREE (Bock et al., 1994; Lev et al., 1999).

sedimentary rocks is rather constant and ranges between 1.0 and 2.0 (McLennan et al., 1993). Adding even a small amount of monazite can result in a significant increase of Gd_N/Yb_N in the sediment (McLennan et al., 1993). Monazite is a phosphate mineral with high LREE content (Deer et al., 1992) and commonly between 0.5 and 4 % Gd_2O_3 (Lee and Bastron, 1967; Milodowski and Zalasiewicz, 1991; Catlos and Miller, 2017; Lazareva et al., 2018). In case of monazite enrichment, one would expect elevated LREE (especially Ce) and Gd in the absolute element abundances of these samples which is not the case (Table 2). Because all groups show similar PAAS-normalized LREE (Fig. 6) but only P2 shows depletion in HREE, which can be most conveniently explained by a missing HREE component, i.e. zircon. This leads to high Gd_N/Yb_N in four out of five P2 samples (see inset in Fig. 7b) and reflects source area characteristics.

5.3. $^{147}Sm-^{143}Nd$ isotopic data

For all samples, the negative εNd(T) values (−6.00 to −21.04; Table 3) calculated for the mudstones indicate a dominant input of terrigenous detritus with an old continental crust affinity (Fig. 8). P3 samples seem to have some contributions from minor juvenile sources,
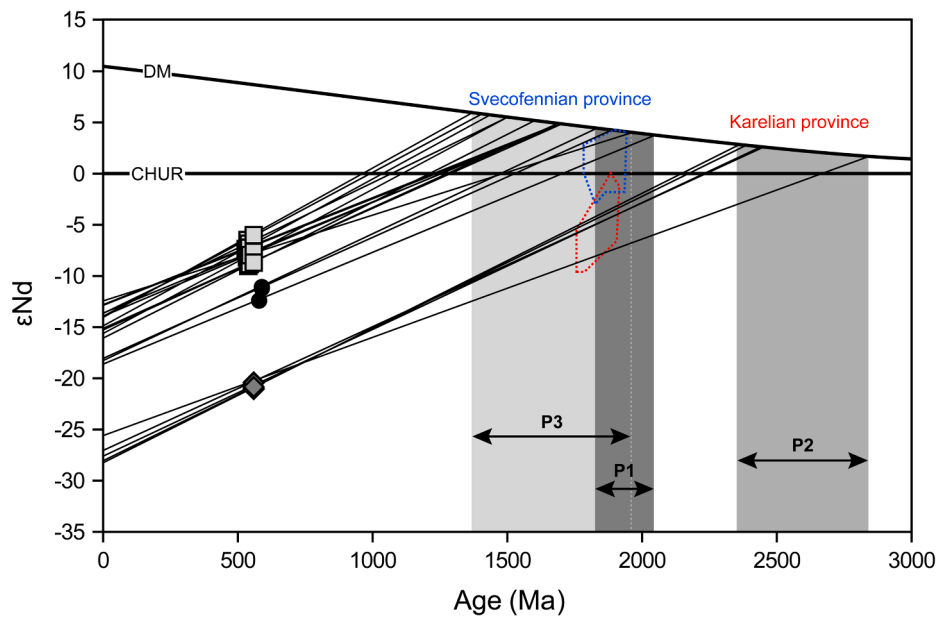
Fig. 9. (a) Nd isotopic composition versus age diagram for mudstones analysed in this study. Crustal residence ages (T_{DM}) (Table 3) define three populations, labelled P1, P2, and P3 (see Section 5.3 for discussion). DM – Depleted mantle evolution model from Nägler and Kramers (1998), CHUR – chondritic uniform reservoir. Reference fields for the Nd isotopic composition of the Karelian and Svecofennian provinces are after Huhma et al. (2011).
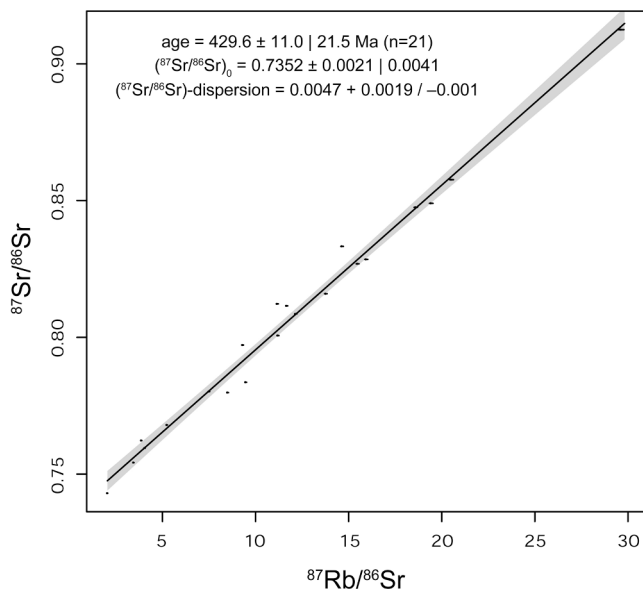
Fig. 10. Rb–Sr whole-rock isochron diagram for mudstones analysed in this study, produced using IsoplotR (Vermeesch, 2018). Overdispersion is attributed to the geological scatter in the ages or in the non-radiogenic isotope composition.

as these samples show the least negative $\varepsilon_{Nd}(T)$ values. The vertical variation in $f_{Sm/Nd}$ within one population of samples (Fig. 8) can be explained by LREE enrichment and depletion, respectively, during crustal formation of the source lithologies (Bock et al., 1994; Lev et al., 1999). Calculated Sm–Nd depleted mantle (DM) crustal residence times (T_{DM}) of siliciclastic sedimentary rocks can be considered as a weighted average of the age and provenance of the eroded rock units in the source area (e.g., O'Nions et al., 1983; Goldstein et al., 1984; McLennan and Hemming, 1992). For the studied mudstones of the Digermulen Peninsula, T_{DM} crustal residence ages confirm the input of detrital material from old continental crust (Fig. 9). Present-day distribution of basement rocks is only an approximation of that during the time of deposition of

the studied sediments as erosion took place since late Ediacaran times. Nevertheless, assuming that the majority of the detrital material was derived from the Fennoscandian Shield of the East European Craton (Fig. 11), possible source areas can be deciphered based on their geochronological ages and Nd isotopic composition.

P1 samples, including the Nyborg and Mortensnes formations, yield mid-Palaeoproterozoic T_{DM} crustal residence ages (Fig. 9). These, together with the negative $\varepsilon_{Nd}(T)$ values, reflect the isotopic signatures of felsic igneous rocks from the Svecofennian province (Figs. 9, 11). Such provenance is supported by palaeocurrent data (Fig. 3), suggesting sediment transport largely from the south (present-day coordinates). Besides, a possible sediment supply from the Svecofennian province is also supported by the fact that detrital zircon U–Pb ages from a sandstone sample of the Nyborg Formation from the adjacent Varanger Peninsula show mainly mid-Palaeoproterozoic ages (Roberts and Siedlecka, 2012).

P2 samples, the oldest part of the Indreelva Member, yield notably older crustal residence ages (T_{DM}) (Fig. 9) that reflect sediment supply from mainly early Palaeoproterozoic and locally Neoarchean rock units. The sediment source must be sought in the Karelian province (Figs. 9, 11). Thus, in a very broad picture, P1 sediment, deposited during a glacial interval, has a more distal source compared to P2 sediment, deposited in post-glacial time, with a more proximal source.

The remaining sedimentary succession (P3), starting from about 2 m below the stratigraphically lowest occurrence of discoidal Ediacara-type fossils to the Lower Breidvika member, yields late Palaeoproterozoic to early Mesoproterozoic crustal residence ages (T_{DM}) (Fig. 9). P3 sediment received detrital material from upper Palaeoproterozoic to lower Mesoproterozoic upper crustal rocks of the Svecofennian province, probably including a lot of recycled clastic sediment, and in addition likely with mixing of juvenile detrital material as the P3 samples have the least negative $\varepsilon_{Nd}(T)$ values (Fig. 8). Such juvenile detrital material may come from young (volcanic) rocks. This is supported by the fact that detrital zircon U–Pb ages from uppermost Ediacaran and lower Cambrian sandstones on the mainland of northern Norway show evidence for mixed sediment influx from old upper crustal sources from the Svecofennian province and juvenile detrital material (ca. 550–570 Ma), the latter being interpreted to be derived from magmatic rocks of the Timanides (Andresen et al., 2014; Zhang et al., 2015). Overall,
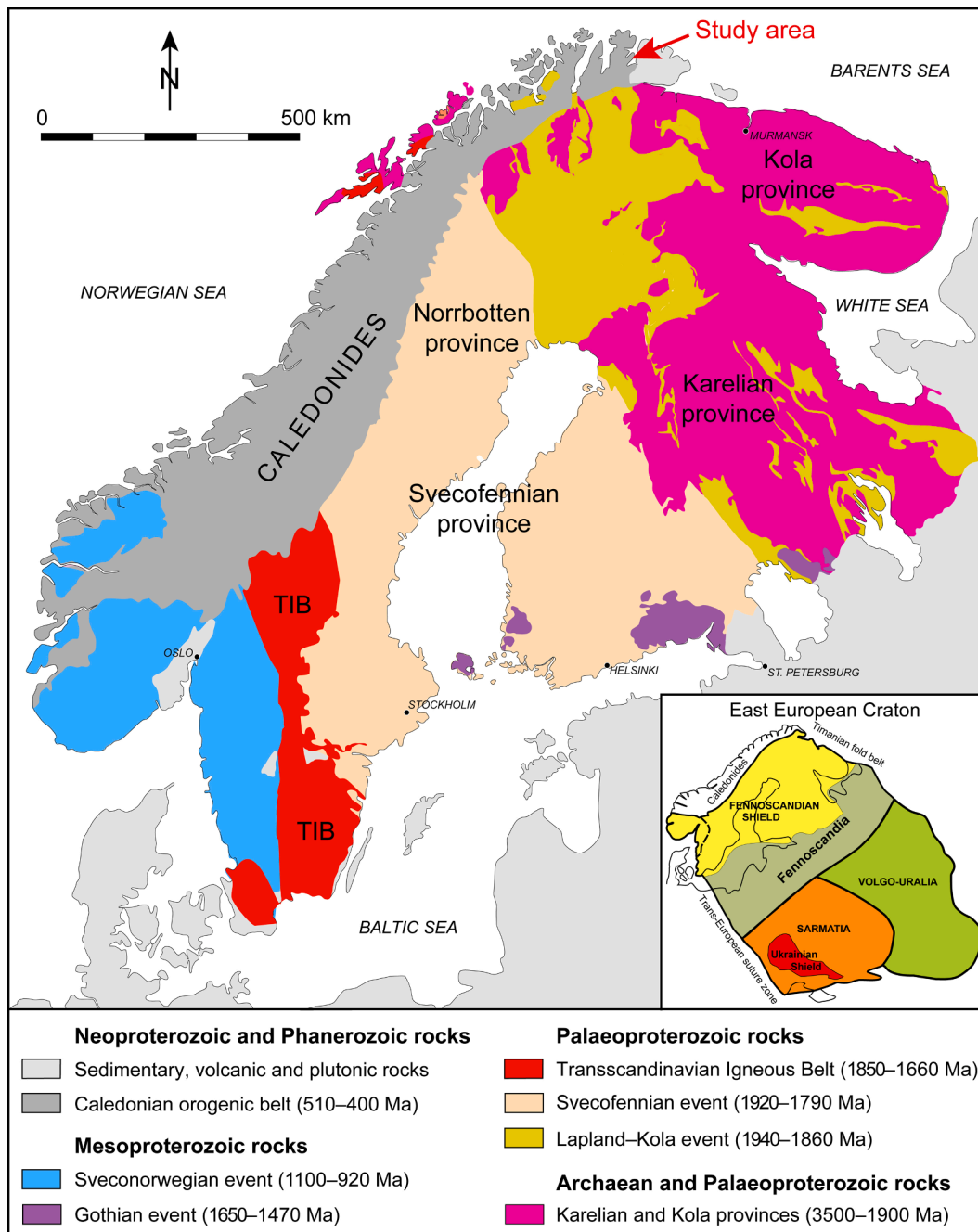
Fig. 11. Geological age provinces of the Fennoscandian Shield (after Lahtinen, 2012), with the simplified geological map based on Koistinen et al. (2001) and insert map based on Gorbatschev and Bogdanova (1993). TIB – Transscandinavian Igneous Belt.

significant shifts in Sm–Nd isotope values obtained from mudstones of the Digermulen Peninsula are in agreement with published detrital zircon dates from sandstones of northern Norway (Roberts and Siedlecka, 2012; Andresen et al., 2014; Zhang et al., 2015), reveal prominent changes in sediment sources (Fig. 12), probably related to large-scale palaeotectonic reorganisation along the Iapetus-facing margin of Baltica during late Neoproterozoic and early Cambrian times.

5.4. ^{87}Rb–^{87}Sr isotopic data

The combined Rb–Sr isotopic data of all samples yield an errorchron age of about 430 Ma (Fig. 10). This is consistent with resetting of the Rb–Sr whole-rock isotope systems of the mudstones during a known tectono-metamorphic event in the Gaissa Nappe Complex of Finnmark

(Dallmeyer et al., 1989), likely representing the peak of metamorphism and cleavage generation on the Digermulen Peninsula. Nonetheless, interpreting Rb–Sr isotope data in sedimentary rocks is highly speculative because of the mobility of Rb and Sr even during diagenetic processes. Previous geochronological data (^{40}Ar/^{39}Ar, K–Ar, Rb–Sr) of whole-rock from the Gaissa Nappe Complex are not easily gauged and have remained controversial (Sundvoll and Roberts, 2003). In Norway, late Silurian–Early Devonian metamorphic ages are related to the continental collision between Baltica and Laurentia and the closure of the Iapetus Ocean, the so-called Scandian phase of the Caledonian Orogeny (Gee, 1975; Roberts, 2003). In Finnmark, about 431–428 Ma-old metamorphic ages are related to main phase of the Scandian Orogeny before gravitationally driven collapse of the orogen (Kirkland et al., 2006). The Rb–Sr age obtained in this study overlaps in error with a
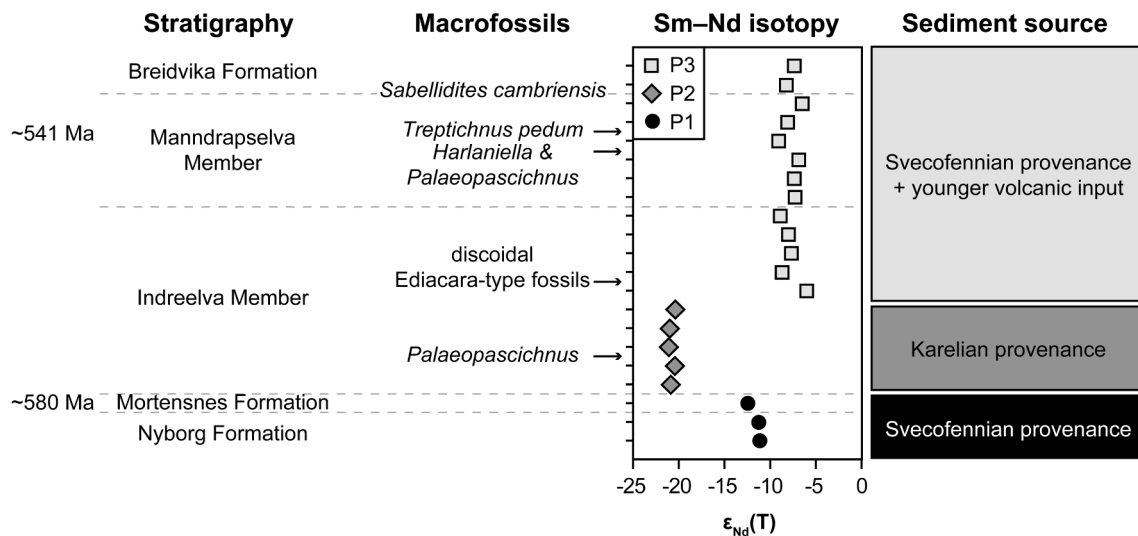
Fig. 12. Summary figure showing the stratigraphy of the studied mudstones from the Digermulen Peninsula, the first occurrences of some prominent macrofossils, the obtained εNd(T) values, and the suggested sediment sources. The three populations, labelled P1, P2, and P3, are explained in Sections 4 and 5.

calcite U–Pb age of 418 ± 23 Ma from deformed cone-in-cone calcite within the 2nd cycle of the Manndrapselva Member on the Digermulen Peninsula (Meinhold et al., 2020). It also overlaps in error with a Rb–Sr age of 430 ± 11 Ma from the<0.1 μm grain-size fraction from the Indreelva Member of the parautochthonous units on the Varanger Peninsula (Gorokhov et al., 2001). However, the Rb–Sr ages are about 30–40 Ma older than K–Ar ages of 403.9 ± 4.2 and 391.5 ± 4.0 Ma from the < 2 and < 0.2 μm grain-size fractions, respectively, of the upper Indreelva Member on the Digermulen Peninsula; these ages have been interpreted to present a thermal overprint under low epizonal conditions along a localised shear zone during the late stage of the Scandian Orogeny (Meinhold et al., 2019b). In summary, at least two tectono-metamorphic phases affected the sedimentary rocks from the Digermulen Peninsula in Finnmark: the main phase and the late phase of the Scandian Orogeny.

6. Implications for Ediacaran biological evolution

Macroscopic metazoans could only have evolved once permissive levels of seawater oxygen had been established, though it is unclear by what time such conditions were reached and how stable they were. However, it has to be factored in that early metazoans – some found among the Ediacara biota – may have had a high tolerance to low oxygen concentrations under which they evolved, as do some modern animals (for instance, sponges; Mills et al., 2014). This notwithstanding, it is generally assumed that the abundance and increase in complexity of the Ediacara biota is related to increased oxygen levels (Sperling et al., 2016; Evans et al., 2018). In most models, an increase in seawater oxygenation significantly precedes the appearance of animals in the fossil record. However, Shi et al. (2022) found evidence that oceanic oxygenation coincided with the Shuram excursion – the largest known negative carbon isotopic excursion in Earth's history that occurred between 574.0 ± 4.7 Ma and 567.3 ± 3.0 Ma (Rooney et al., 2020) – approximating the appearance of the earliest Ediacara biota. Recent studies suggest modest and fluctuating oxygen levels during the Ediacaran Period (e.g., Tostevin and Mills 2020), which may have controlled the distribution of animals (e.g., Li et al., 2015; Cui et al., 2016).

Distribution of the Ediacaran macrofossils in successions in China, Namibia and Siberia is largely controlled by the redox state of the water column (e.g., McFadden et al., 2008; Wood et al., 2015; Bowyer et al., 2017). Large and complex organisms, especially taxa of the earliest mobile metazoans may have had metabolic demands for dissolved

oxygen concentration higher than during most of the Precambrian (e.g., Sperling et al., 2013; Tostevin et al., 2016b). Along these lines, Evans et al. (2018), based on data from South China, concluded that the appearance of morphologically complex Ediacara-type fossils of the White Sea association (approximately 560–551 Ma) coincided with increased seawater oxygen levels. They also suggested that the lower diversity in the succeeding Nama assemblage (approximately 551–540 Ma) coincided with, and was caused by, a decrease in oxygen levels. Zhang et al. (2019) found evidence for an earlier appearance in the rise of seawater oxygen but similarly found evidence for increased sea-floor anoxia at the terminal part of the Ediacaran. The terminal Ediacaran decline in biotic diversity on the East European Platform has been called the 'Kotlinian Crisis' (Kolesnikov et al., 2015). Grazhdankin (2014) attributed this decline to the rise of mobile bilaterians and no evidence was detected for environmental changes and bottom water redox conditions remained unchanged through the biotic change recorded on the East European Platform (see Maslov et al., 2019).

We compared the sedimentological evidence for the change in oxygenation state of the bottom water with the fossil record observed in the older strata of the Stáhpogieddi Formation (mainly lower part of the Indreelva Member) to see whether environmental conditions may have been important for early macroscopic life on Baltica. Proxy results from P2 and some P3 mudstones suggest that the earliest appearance of macroscopic fossils in the basal part of the Indreelva Member (e.g., palaeopascichnids and probable metazoan Ediacara-type fossils) in Finnmark/Scandinavia (Högström et al., 2013; Jensen et al., 2018b) was associated with sediment deposition in a well-oxygenated environment. This interval is probably younger than approximately 560 Ma (Jensen et al., 2018b), so temporarily belongs to the White Sea association. The differences in the fossil assemblages between the two principal fossiliferous levels in the Indreelva Member can be attributed to facies. The Indreelva Member has been classified as an example of Fermeuse-style preservation which characterizes deeper water settings in which microbial mats were not normally formed reducing the preservation of surficial fossils, with a predominance of *Aspidella* discs formed in the sediment (Narbonne, 2005). Specimens of *Aspidella* in the lower Indreelva Member (Fig. 4a) are associated with the appearance of thin sandstone beds. These *Aspidella* often show a depth of several centimetres, are consistent with an organism's partial emplacement in the sediment. The more diverse assemblage of fossils typical of the White Sea assemblage higher in the Indreelva Member (Fig. 4b) is attributed to a facies more conducive to their preservation.

The results from redox-sensitive elements presented in this paper allow evaluating the role of the oxygenation state of the bottom water on the distribution of macroscopic fossils. The onset of oxic depositional conditions observed in the P3 sediments coincides with the occurrence of the Ediacara-type biota. Our data further suggest bottom water oxygenation for the latest Ediacaran of the Manndrapselva Member and the top of the Indreelva Member. This part of the succession yields palaeopascichnids (Fig. 4c) but metazoan Ediacara-type fossils have not been found. Trace fossils are prominent in the Ediacaran middle part of the Manndrapselva Member (McIlroy and Brasier, 2017; Jensen et al., 2018b), typical of the Nama-type time-equivalent associations elsewhere (e.g., Darroch et al., 2021). Our results are similar to those of earlier studies from the East European Platform (Johnston et al., 2012; Maslov et al., 2019) in suggesting oxic seafloor conditions during the Ediacaran, suggesting that other factors likely were more important for the pattern of biotic changes, such as nutrients (e.g., Pehr et al., 2018), competition (Grazhdankin, 2004), or inevitable outcomes of evolutionary processes (cf. Budd and Mann, 2020). On the other hand, the shift in sediment provenance, i.e. change in lithological composition of the source area(s), between P1, P2 and P3 is probably not responsible for the diversity and composition of fossil assemblages. For example, palaeopascichnids occur in P2 and P3 sediments. However, the shift in sediment provenance may have influenced the sedimentation rate or the depositional setting, which would have an impact on the preservation of fossils.

7. Conclusions

The analyses of the Nd and Sr isotopic and REE composition of the fossil-bearing Ediacaran and lowermost Cambrian succession of the Digermulen Peninsula, Arctic Norway, provide first constraints on the provenance and post-depositional alteration of these strata. Our study shows that:

1) All studied samples are argillaceous mudstones. They are carbonate-free, with the exception of small amounts in a single sample from the glaciogenic Mortensnes Formation.

2) Mudstones from the Nyborg and Mortensnes formations do not display any Ce anomaly. They yield mid-Palaeoproterozoic T_{DM} crustal residence ages, and together with the negative $\varepsilon_{Nd}(T)$ values reflect the isotopic signatures of felsic igneous from the Svecofennian province.

3) The lowermost five samples from the Indreelva Member display true negative Ce anomalies, and thus sediments were deposited under well-oxygenated seafloor conditions. Their crustal residence ages (T_{DM}) reflect sediment supply from mainly early Paleoproterozoic and locally Neoarchean rock units, as present in the Karelian province.

4) Samples starting about 2 m below the stratigraphically lowest occurrence of discoidal Ediacara-type fossils to the Lower Breidvika member show varying Ce anomalies. Their negative $\varepsilon_{Nd}(T)$ and T_{DM} values suggest sediment supply from upper Palaeoproterozoic to lower Mesoproterozoic upper crustal rocks of the Svecofennian province, and in addition likely some juvenile (late Neoproterozoic volcanic) source.

5) Shifts in Sm–Nd isotope values from the glacial to the post-glacial succession and within the post-glacial succession, approximately 2 m below the first appearance of macroscopic Ediacara-type fossils of probable metazoans, are related to changes in the sediment source and probably to large-scale palaeotectonic reorganisation along the Iapetus-facing margin of Baltica.

6) The combined Rb–Sr isotopic data of all samples yield an errorchron age of about 430 Ma reflecting the resetting of the Rb–Sr whole-rock isotope systems of the mudstones during a Scandian tectono-metamorphic event in the Gaissa Nappe Complex of Finnmark.

7) The earliest appearance of macroscopic fossils in Finnmark/Scandinavia was associated with sediment deposition in a well-oxygenated environment.

References

Agić, H., Högström, A.E.S., Moczydłowska, M., Jensen, S., Palacios, T., Meinhold, G., Ebbestad, J.O.R., Taylor, W.L., Høyberget, M., 2019. Organically-preserved multicellular eukaryote from the early Ediacaran Nyborg Formation, Arctic Norway. Scientific Reports 9, article number: 14659. https://doi.org/10.1038/s41598-019-50650-x.

Agić, H., Högström, A.E.S., Jensen, S., Ebbestad, J.O.R., Vickers-Rich, P., Hall, M., Matthews, J.J., Meinhold, G., Høyberget, M., Taylor, W.L., 2022. Late Ediacaran occurrences of the organic-walled microfossils *Granomarginata* and flask-shaped *Lagoenaforma collaris* gen. et sp. nov. Geological Magazine 157, 1071–1092. https://doi.org/10.1017/S0016756821001096.

Alibo, D.S., Nozaki, Y., 1999. Rare earth elements in seawater: particle association, shale-normalization, and Ce oxidation. Geochimica et Cosmochimica Acta 63, 363–372.

Allègre, C.J., Rousseau, D., 1984. The growth of the continent through geological time studied by Nd isotope analysis of shales. Earth and Planetary Science Letters 67, 19–34.

Anderson, T., 2014. Key parameters for liquid-rich unconventional plays: case studies from North America. AAPG Search Discovery Article #80354.

Andresen, A., Agyei-Dwarko, N.Y., Kristoffersen, M., Hanken, N.-M., 2014. A Timanian foreland basin setting for the late Neoproterozoic – Early Palaeozoic cover sequences (Dividal Group) of northeastern Baltica. In: Corfu, F., Gasser, D., Chew, D.M. (Eds.), New perspectives on the Caledonides of Scandinavia and related Areas. Geological Society, London, Special Publication 390, 157–175.

Arndt, N.T., Goldstein, S.L., 1987. Use and abuse of crust-formation ages. Geology 15, 893–895.

Awasthi, N., Ray, E., Paul, D., 2018. Sr and Nd isotope compositions of alluvial sediments from the Ganga Basin and their use as potential proxies for source identification and apportionment. Chemical Geology 476, 327–339.

Awwiller, D.N., Mack, L.E., 1991. Diagenetic modification of Sm–Nd model ages in Tertiary sandstones and shales, Texas Gulf Coast. Geology 19, 311–314.

Banks, N.L., 1973. Innerelv Member: late Precambrian marine shelf deposit, east Finnmark. Norges Geologiske Undersøkelse 288, 7–25.

Banks, N.L., Edwards, M.B., Geddes, W.P., Hobday, D.K., Reading, H.G., 1971. Late Precambrian and Cambro-Ordovician sedimentation in East Finnmark. Norges Geologiske Undersøkelse 269, 197–236.

Bau, M., Dulski, P., 1996. Distribution of yttrium and rare-earth elements in the Penge and Kuruman iron-formations, Transvaal Supergroup, South Africa. Precambrian Research 79, 37–55.

Belousova, E.A., Walters, S., Griffin, W.L., O'Reilly, S.Y., Fisher, N.I., 2002. Zircon trace-element compositions as indicators of source rock type. Contributions to Mineralogy and Petrology 143, 602–622.

Bhandari, N., Shukla, P.N., Ghevariya, Z.G., Sundaram, S.M., 1996. K/T boundary layer in Deccan Intertrappeans at Anjar, Kutch. In: Ryder, G., Fastovsky, D.E., Garner, S. (Eds.), The Cretaceous-Tertiary event and other catastrophes in Earth History. Geological Society of America, Special Paper 307, 417–424.

Bock, B., McLennan, S.M., Hanson, G.N., 1994. Rare earth elements redistribution and its effects on the neodymium isotope system in the Austin Glen Member of the Normenskill Formation, New York, USA. Geochimica et Cosmochimica Acta 58, 5245–5253.

Bock, B., McLennan, S.M., Hanson, G.N., 1998. Geochemistry and provenance of the Middle Ordovician Austin Glen Member (Normanskill Formation) and the Taconian Orogeny in New England. Sedimentology 45, 635–655.

Boelrijk, N.A.I.M., 1968. A general formula for "double" isotope dilution analysis. Chemical Geology 3, 323–325.

Bouvier, A., Vervoort, J.D., Patchett, P.J., 2008. The Lu–Hf and Sm–Nd isotopic composition of CHUR: Constraints from unequilibrated chondrites and implications for the bulk composition of terrestrial planets. Earth and Planetary Science Letters 273, 48–57.

Bowyer, F., Wood, R.A., Poulton, S.W., 2017. Controls on the evolution of Ediacaran metazoan ecosystems: A redox perspective. Geobiology 15, 516–551.

Budd, G.E., Mann, R.P., 2020. The dynamic of stem and crown groups. Science Advances 6, article number: eaaz1626. DOI:10.1126/sciadv.aaz1626.

Catlos, E.J., Miller, N.R., 2017. Speculations linking monazite compositions to origin: Llallagua tin ore deposit (Bolivia). Resources 6, article number: 36. https://doi.org/10.3390/resources6030036.

Cohen, K.M., Harper, D.A.T., Gibbard, P.L., Fan, J.-X., 2021. The International Chronostratigraphic Chart. International Commission on Stratigraphy.

Compston, W., Pidgeon, R.T., 1962. Rubidium-strontium dating of shales by the total-rock method. Journal of Geophysical Research 67, 3493–3502.

Condie, K.C., 1991. Another look at rare earth elements in shales. Geochimica et Cosmochimica Acta 55, 2527–2531.

Cui, H., Grazhdankin, D.V., Xiao, S., Peek, S., Rogov, V.I., Bykova, N.V., Sievers, N.E., Liu, X.-M., Kaufman, A.J., 2016. Redox-dependent distribution of early macro-organisms: Evidence from the terminal Ediacaran Khatyspyt Formation in Arctic Siberia. Palaeogeography, Palaeoclimatology, Palaeoecology 461, 122–139.

Cullers, R.L., 1995. The controls on the major- and trace-element evolution of shales, siltstones and sandstones of Ordovician to Tertiary age in the Wet Mountains region, Colorado, U.S.A. Chemical Geology 123, 107–131.

Cullers, R.L., Chaudhuri, S., Arnold, B., Lee, M., Wolf Jr., C.W., 1975. Rare-earth distributions in clay minerals and clay-sized fractions of lower Permian Havensville and Eskridge shales of Kansas and Oklahoma. Geochimica et Cosmochimica Acta 39, 1691–1703.

Cunningham, J.A., Liu, A.G., Bengtson, S., Donoghue, P.C.J., 2017. The origin of animals: Can molecular clocks and the fossil record be reconciled? BioEssays 39, article number: 1600120. https://doi.org/10.1002/bies.20160012.

Dallmeyer, R.D., Reuter, A., Clauer, N., Leiwig, N., 1989. Chronology of Caledonian tectonothermal activity within the Gaissa and Laksefjord Nappe Complexes (Lower Allochthon), Finnmark, Norway: evidence from K-Ar and ^{40}Ar/^{39}Ar ages. In: Gayer, R.A. (Ed.), The Caledonide geology of Scandinavia. Graham & Trotman, London, pp. 9–26.

Darroch, S.A.F., Cribb, A.T., Buatois, L.A., Germs, G.J.B., Kenchington, C.G., Smith, E.F., Mocke, H., O'Neil, G.R., Schiffbauer, J.D., Maloney, K.M., Racicot, R.A., Turk, K.A., Gibson, B.M., Almond, J., Koester, B., Boag, T.H., Tweedt, S.M., Laflamme, M., 2021. The trace fossil record of the Nama Group, Namibia: Exploring the terminal Ediacaran roots of the Cambrian explosion. Earth-Science Reviews 212, article number: 103435. https://doi.org/10.1016/j.earscirev.2020.103435.

Deer, W.A., Howie, R.A., Zussman, J., 1992. An Introduction to Rock-Forming Minerals, 2nd edition. Longman Group Ltd, Harlow, UK, p. 712.

DePaolo, D.J., 1981. A neodymium and strontium isotopic study of the Mesozoic calc-alkaline granitic batholiths of the Sierra Nevada and Peninsular Ranges, California. Journal of Geophysical Research 86, 10470–10488.

DePaolo, D.J., Wasserburg, G.J., 1976. Nd isotopic variations and petrogenetic models. Geophysical Research Letters 3, 249–252.

Dittmar, T., Hertkorn, N., Kattner, G., Lara, R.J., 2006. Mangroves, a major source of dissolved organic carbon to the oceans. Global Biogeochemical Cycles 20, GB1012. https://doi.org/10.1029/2005GB002570.

Ebbestad, J.O.R., Hybertsen, F., Högström, A.E.S., Jensen, S., Palacio, T., Taylor, W.L., Agić, H., Høyberget, M., Meinhold, G., 2022. Distribution and correlation of *Sabellidites cambriensis* (Annelida?) in the basal Cambrian on Baltica. Geological Magazine 159, 1262–1283. https://doi.org/10.1017/S0016756821001187.

Elderfield, H., Greaves, M.J., 1982. The rare earth elements in seawater. Nature 296, 214–219.

Evans, S.D., Diamond, C.W., Droser, M.L., Lyons, T.W., 2018. Dynamic oxygen and coupled biological and ecological innovation during the second wave of the Ediacara biota. Emerging Topics in Life Sciences 2, 223–233.

Farmer, J., Vidal, G., Moczydłowska, M., Strauss, H., Ahlberg, P., Siedlecka, A., 1992. Ediacaran fossils from the Innerelv Member (late Proterozoic) of the Tanafjorden area, northeastern Finnmark. Geological Magazine 129, 181–195.

Gao, S., Wedepohl, K.H., 1995. The negative Eu anomaly in Archean sedimentary rocks: Implication for decomposition and age and importance of their granitic sources. Earth and Planetary Science Letters 133, 81–94.

Gebauer, D., Grünenfelder, M., 1974. Rb-Sr whole rock dating of late diagenetic to anchimetomorphic, Paleozoic sediments in Southern France (Montague Noire). Contributions to Mineralogy and Petrology 47, 113–130.

Gee, D.G., 1975. A tectonic model for the central part of the Scandinavian Caledonides. American Journal of Science 275, 468–515.

Goldstein, S.L., O'Nions, R.K., Hamilton, P.J., 1984. A Sm-Nd isotopic study of atmospheric dusts and particulates from major river systems. Earth and Planetary Science Letters 70, 221–236.

Gorbatschev, R., Bogdanova, S., 1993. Frontiers in the Baltic Shield. Precambrian Research 64, 3–21.

Gorokhov, I.M., Siedlecka, A., Roberts, D., Melnikov, N.M., Turchenko, T.L., 2001. Rb–Sr dating of diagenetic illite in Neoproterozoic shales, Varanger Peninsula, Northern Norway. Geological Magazine 138, 541–562.

Grazhdankin, D., 2004. Patterns of distribution in the Ediacaran biotas: facies versus biogeography and evolution. Paleobiology 30, 203–221.

Grazhdankin, D., 2014. Patterns of evolution of the Ediacaran soft-bodied biota. Journal of Paleontology 88, 269–283.

Hegner, E., Walter, H.J., Satir, M., 1995. Pb-Sr-Nd isotopic compositions and trace element geochemistry of megacrysts and melilitites from the Tertiary Urach volcanic field: source composition of small volume melts under SW Germany. Contributions to Mineralogy and Petrology 122, 322–335.

Hegner, E., Klemd, R., Kröner, A., Corsini, M., Alexeiev, D.V., Iaccheri, L.M., Zack, T., Dulski, P., Xia, X., Windley, B.F., 2010. Mineral ages and P-T conditions of Late Paleozoic high-pressure eclogite and provenance of mélange sediments. American Journal of Science 110, 916–950.

Högström, A.E.S., Jensen, S., Palacios, T., Ebbestad, J.O.R., 2013. New information on the Ediacaran-Cambrian transition in the Vestertana Group, Finnmark, northern Norway, from trace fossils and organic-walled microfossils. Norwegian Journal of Geology 93, 95–106.

Huhma, H., O'Brien, H., Lahaye, Y., Mänttäri, I., 2011. Isotope geology and Fennoscandian lithosphere evolution. Geological Survey of Finland, Special Paper 49, 35–48.

Jensen, S., Högström, A.E.S., Almond, J., Taylor, W.L., Meinhold, G., Høyberget, M., Ebbestad, J.O.R., Agić, H., Palacios, T., 2018a. Scratch circles from the Ediacaran and Cambrian of Arctic Norway and the Republic of South Africa, with a review of scratch circle occurrences. Bulletin of Geosciences 93, 287–304.

Jensen, S., Högström, A.E.S., Høyberget, M., Meinhold, G., McIlroy, D., Ebbestad, J.O.R., Taylor, W.L., Agić, H., Palacios, T., 2018b. New occurrences of *Palaeopascichnus* from the Stáhpogieddi Formation, Arctic Norway, and their bearing on the age of the Varanger Ice Age. Canadian Journal of Earth Sciences 55, 1253–1261.

Johnston, D.T., Poulton, S.W., Goldberg, T., Sergeev, V.N., Podkovyrov, V., Vorob'eva, N.G., Bekker, A., Knoll, A.H., 2012. Late Ediacaran redox stability and metazoan evolution. Earth Earth and Planetary Science Letters 335–336, 25–35.

Kirkland, C.L., Daly, J.S., Eide, E.A., Whitehouse, M.J., 2006. The structure and timing of lateral escape during the Scandian Orogeny: A combined strain and geochronological investigation in Finnmark, Arctic Norwegian Caledonides. Tectonophysics 425, 159–189.

Koistinen, T., Stephens, M.B., Bogatchev, V., Nordgulen, Ø., Wennerström, M., Korhonen, J., 2001. Geological map of the Fennoscandian Shield, scale 1:2 000 000. Geological Surveys of Finland, Norway and Sweden and the Northwest Department of the Natural Resources of Russia.

Kolesnikov, A., Desiatkin, V., 2022. Taxonomy and palaeoenvironmental distribution of palaeopascichnids. Geological Magazine 159, 1175–1191.

Kolesnikov, A.V., Marusin, V.V., Nagovitsin, K.E., Maslov, A.V., Grazhdankin, D.V., 2015. Ediacaran biota in the aftermath of the Kotlinian Crisis: Asha Group of the South Urals. Precambrian Research 263, 59–78.

Kumpulainen, R.A., Hamilton, M.A., Söderlund, U., Nystuen, J.P., 2021. U-Pb baddeleyite age for the Ottfjället Dyke Swarm, central Scandinavian Caledonides: new constraints on Ediacaran opening of the Iapetus Ocean and glaciations on Baltica. GFF 143, 40–54.

Lahtinen, R., 2012. Main geological features of Fennoscandia. Geological Survey of Finland, Special Paper 53, 13–18.

Lazar, O.R., Bohacs, K.M., Macquaker, J.H.S., Schieber, J., Demko, T.M., 2015. Capturing key attributes of fine-grained sedimentary rocks in outcrops, cores, and thin sections: nomenclature and description guidelines. Journal of Sedimentary Research 85, 230–246.

Lazareva, E.V., Zhmodik, S.M., Prokopiev, A.V., Karmanov, N.S., Sergeenko, A.I., 2018. Nodular monazite from placers in the Kular Ridge (Arctic Siberia, Russia): composition and age. Russian Geology and Geophysics 59, 1330–1347.

Lee, D.E., Bastron, H., 1967. Fractionation of rare-earth elements in allanite and monazite as related to geology of the Mt. Wheeler mine area. Nevada. Geochimica et Cosmochimica Acta 31, 339–356.

Lev, S.M., McLennan, S.M., Hanson, G.N., 1999. Mineralogic control on REE mobility during black-shale diagenesis. Journal of Sedimentary Research 69, 1071–1082.

Li, C., Planavsky, N.J., Shi, W., Zhang, Z., Zhou, C., Cheng, M., Tarhan, L.G., Luo, G., Xie, S., 2015. Ediacaran marine redox heterogeneity and early animal ecosystems. Scientific Reports 5, article number: 17097. https://doi.org/10.1038/srep17097.

Lugmair, G.W., Marti, K., 1978. Lunar initial ^{143}Nd/^{144}Nd: differential evolution of the lunar crust and mantle. Earth and Planetary Science Letters 39, 349–357.

Maslov, A.V., Grazhdankin, D.V., Podkovyrov, V.N., 2019. Late Vendian Kotlinian Crisis on the East European Platform: Lithogeochemical indicators of depositional environment. Lithology and Mineral Resources 54, 1–26.

McCulloch, M.T., Wasserburg, G.J., 1978. Sm-Nd and Rb-Sr chronology of continental crust formation. Science 200, 1003–1011.

McIlroy, D., Brasier, M.D., 2017. Ichnological evidence for the Cambrian explosion in the Ediacaran to Cambrian succession of Tanafjord, Finnmark, northern Norway. In: Brasier, A.T., McIlroy, D., McLoughlin, N. (Eds.), Earth System Evolution and Early Life: a Celebration of the Work of Martin Brasier. Geological Society, London, Special Publication 448, pp. 351–368.

McLennan, S.M., 1989. Rare earth elements in sedimentary rocks: influence of provenance and sedimentary processes. Reviews in Mineralogy 21, 169–200.

McLennan, S.M., Hemming, S.R., 1992. Samarium/neodymium elemental and isotopic systematics in sedimentary rocks. Geochimica et Cosmochimica Acta 56, 887–898.

McLennan, S.M., Taylor, S.R., McCulloch, M.T., Maynard, J.B., 1990. Geochemical and Nd-Sr isotopic composition of deep-sea turbidites: Crustal evolution and plate tectonic associations. Geochimica et Cosmochimica Acta 54, 2015–2050.

McLennan, S.M., Hemming, S., McDaniel, D.K., Hanson, G.N., 1993. Geochemical approaches to sedimentation, provenance, and tectonics. In: Johnsson, M.J., Basu, A. (Eds.), Processes Controlling the Composition of Clastic Sediments. Geological Society of America, Special Paper 284, 21–40.

Meinhold, G., Jensen, S., Høyberget, M., Arslan, A., Ebbestad, J.O.R., Högström, A.E.S., Palacios, T., Agić, H., Taylor, W.L., 2019a. First record of carbonates with spherulites and cone-in-cone structures from the Precambrian of Arctic Norway, and their palaeoenvironmental significance. Precambrian Research 328, 99–110.

Meinhold, G., Wemmer, K., Högström, A.E.S., Ebbestad, J.O.R., Jensen, S., Palacios, T., Høyberget, M., Agić, H., Taylor, W.L., 2019b. A late Caledonian tectono-thermal event in the Gaissa Nappe Complex, Arctic Norway: fine-fraction K-Ar evidence from the Digermulen Peninsula. GFF 141, 289–294.

Meinhold, G., Roberts, N.M.W., Arslan, A., Jensen, S., Ebbestad, J.O.R., Högström, A.E. S., Høyberget, M., Agić, H., Palacios, T., Taylor, W.L., 2020. U-Pb dating of calcite in ancient carbonates for age estimates of syn- to post-depositional processes: a case study from the upper Ediacaran strata of Finnmark, Arctic Norway. Geological Magazine 157, 1367–1372.

Mills, D.B., Ward, L.M., Jones, C., Sweeten, B., Forth, M., Treusch, A.H., Canfield, D.E., 2014. Oxygen requirements of the earliest animals. Proceedings of the National Academy of Sciences 111, 4168–4172.

Milodowski, A.E., Zalasiewicz, J.A., 1991. Redistribution of rare earth elements during diagenesis of turbidite/hemipelagite mudrock sequences of Llandovery age from central Wales. In: Morton, A.C., Todd, S.P., Haughton, P.D.W. (Eds.), Developments in Sedimentary Provenance Studies. Geological Society, London, Special Publication 57, 101–124.

Nägler, T.F., Kramers, J.D., 1998. Nd isotopic evolution of the upper mantle during the Precambrian: models, data and the uncertainty of both. Precambrian Research 91, 233–252.

Narbonne, G.M., 2005. The Ediacara biota: Neoproterozoic origin of animals and their ecosystems. Annual Reviews of Earth and Planetary Sciences 33, 421–442.

Nath, B.N., Bau, M., Rao, B.R., Rao, C.M., 1997. Trace and rare earth elemental variation in Arabian Sea sediments through a transect across the oxygen minimum zone. Geochimica et Cosmochimica Acta 61, 2375–2388.

Nystuen, J.P., 1985. Facies and preservation of glaciogenic sequences from the Varanger ice age in Scandinavia and other parts of the North Atlantic region. Palaeogeography, Palaeoclimatology, Palaeoecology 51, 209–229.

Ohr, M., Halliday, A.N., Peacor, D.R., 1991. Sr and Nd isotopic evidence for punctuated clay diagenesis, Texas Gulf Coast. Earth and Planetary Science Letters 105, 110–126.

O'Nions, R.K., Hamilton, P.J., Hooker, P.J., 1983. A Nd isotope investigation of sediments related to crustal development in the British Isles. Earth and Planetary Science Letters 63, 229–240.

Orem, W.H., Hatcher, P.G., Spiker, E.C., Szeverenyi, N.M., Maciel, G.E., 1986. Dissolved organic matter in anoxic pore waters from Mangrove Lake, Bermuda. Geochimica et Cosmochimica Acta 50, 609–618.

Nelson, B.K., DePaolo, D.J., 1988. Comparison of isotopic and petrographic provenance indicators in sediments from Tertiary continental basins of New Mexico. Journal of Sedimentary Petrology 58, 348–357.

Palacios, T., Ou, Z., Agić, H., Högström, A.E.S., Jensen, S., Høyberget, M., Meinhold, G., Taylor, W.L., Ebbestad, J.O.R., 2017. Organic-walled microfossils and organic fossils across the Ediacaran–Cambrian boundary on the Digermulen Peninsula, Arctic Norway. International Symposium on the Ediacaran–Cambrian transition, 15–29 June 2017, St. John's, Newfoundland, Canada.

Pattan, J.N., Pearce, N.J.G., Mislanker, P.G., 2005. Constraints in using cerium anomaly of bulk sediments as an indicator of paleo bottom water redox environment: a case study from the Central Indian Ocean Basin. Chemical Geology 221, 260–278.

Pease, V., Dovzhakova, E., Beliakova, L., Gee, D.G., 2004. Late Neoproterozoic granitoid magmatism in the Basement to the Pechora Basin, NW Russia: geochemical constraints indicate westward subduction beneath NE Baltica. In: Gee, D.G., Pease, V. (Eds.), The Neoproterozoic Timanide Orogen of Eastern Baltica. Geological Society, London, Memoirs 30, 75–85.

Pehr, K., Love, G.D., Hoffmann, A., Kuznetsov, A., Podkovyrov, V., Junium, C.K., Shumlyanskyy, L., Sokur, T., Bekker, A., 2018. Ediacara biota flourished in oligotrophic and bacterially dominated marine environmenjts across Baltica. Nature Communications 9, article number: 1807. https://doi.org/10.1038/s41467-018-04195-8.

Pettijohn, F.J., 1941. Persistence of heavy minerals and geologic age. Journal of Geology 49, 610–625.

Pin, C., Gannoun, A., Dupont, A., 2014. Rapid, simultaneous separation of Sr, Pb, and Nd by extraction chromatography prior to isotope ratios determination by TIMS and MC-ICP-MS. Journal of Analytical Atomic Spectrometry 29, 1858–1870.

Pourmand, A., Dauphas, N., Ireland, T.J., 2012. A novel extraction chromatography and MC-ICP-MS technique for rapid analysis of REE, Sc and Y: revising CI-chondrite and Post-Archean Australian Shale (PAAS) abundances. Chemical Geology 291, 38–54.

Prasad, M.B.K., Ramanathan, A., 2008. Distribution of rare earth elements in the Pichavaram mangrove sediments of the southeast coast of India. Journal of Coastal Research 24, 126–134.

Pringle, I.R., 1973. Rb-Sr age determinations on shales associated with the Varanger Ice Age. Geological Magazine 109, 465–560.

Pu, J.P., Bowring, S.A., Ramezani, J., Myrow, P., Raub, T.D., Landing, E., Mills, A., Hodgin, E., Macdonald, F.A., 2016. Dodging snowballs: geochronology of the Gaskiers glaciation and the first appearance of the Ediacaran biota. Geology 44, 955–958.

Reading, H.G., 1965. Eocambrian and Lower Palaeozoic geology of the Digermul Peninsula, Tanafjord, Finnmark. Norges Geologiske Undersøkelse 234, 167–191.

Reading, H.G., Walker, R.G., 1966. Sedimentation of Eocambrian tillites and associated sediments in Finnmark, northern Norway. Palaeogeography, Palaeoclimatology, Palaeoecology 2, 177–212.

Rice, A.H.N., 2014. Restoration of the external Caledonides, Finnmark, North Norway. In: Corfu, F., Gasser, D., Chew, D.M. (Eds.), New Perspectives on the Caledonides of Scandinavia and related areas. Geological Society, London, Special Publication 390, 271–299.

Rice, A.H.N., Edwards, M.B., Hansen, T.A., Arnaud, E., Halverson, G.P., 2011. Glaciogenic rocks of the Neoproterozoic Smalfjord and Mortensnes Formations, Vestertana Group, E. Finnmark, Norway. In: Arnaud, E., Halverson, G.P., Shields-Zhou, G. (Eds.), The Geological Record of Neoproterozoic Glaciations. Geological Society, London, Memoir 36, 593–602.

Roberts, D., 2003. The Scandinavian Caledonides: event chronology, palaeogeographic settings and likely modern analogues. Tectonophysics 365, 283–299.

Roberts, D., Siedlecka, A., 2012. Provenance and sediment routing of Neoproterozoic formations on the Varanger, Nordkinn, Rybachi and Sredni peninsulas, North Norway and Northwest Russia: a review. Norges Geologiske Undersøkelse Bulletin 452, 1–19.

Rooney, A.D., Strauss, J.V., Brandon, A.D., Macdonald, F.A., 2015. A Cryogenian chronology: two long-lasting synchronous Neoproterozoic glaciations. Geology 43, 459–462.

Rooney, A.D., Cantine, M.D., Bergmann, K.D., Gómez-Pérez, I., Al Baloushi, B., Boag, T. H., Busch, J.F., Sperling, E.A., Strauss, J.V., 2020. Calibrating the coevolution of Ediacaran life and environment. Proceedings of the National Academy of Sciences 117, 16824–16830.

Roy, M., van de Flierdt, T., Hemming, S.R., Goldstein, S.L., 2007. ^{40}Ar/^{39}Ar ages of hornblende grains and bulk Sm/Nd isotopes of circum-Antarctic glacio-marine sediments: implications for sediment provenance in the southern ocean. Chemical Geology 244, 507–519.

Rubatto, D., 2002. Zircon trace element geochemistry: distribution coefficients and the link between U-Pb ages and metamorphism. Chemical Geology 184, 123–138.

Sahoo, S.K., Planavsky, N.J., Jiang, G., Kendall, B., Owens, J.D., Wang, X., Shi, X., Anbar, A.D., Lyons, T.W., 2016. Oceanic oxygenation events in the anoxic Ediacaran ocean. Geobiology 14, 457–468.

Siedlecka, A., Reading, H.G., Williams, G.D., Roberts, D., 2006. Langfjorden, preliminary bedrock geology map 2236 II, scale 1:50000. Norges Geologiske Undersøkelse, Trondheim.

Shi, W., Mills, B.J.W., Li, C., Poulton, S.W., Krause, A.J., He, T., Zhou, Y., Cheng, M., Shields, G.A., 2022. Decoupled oxygenation of the Ediacaran ocean and atmosphere during the rise of early animals. Earth and Planetary Science Letters 591, article number: 117619. https://doi.org/10.1016/j.epsl.2022.117619.

Shields, G., Stille, P., 2001. Diagenetic constraints on the use of cerium anomalies as palaeoseawater redox proxies: an isotopic and REE study of Cambrian phosphorites. Chemical Geology 175, 29–48.

Shields-Zhou, G.A., Porter, S., Halverson, G.P., 2016. A new rock-based definition for the Cryogenian Period (circa 720–635 Ma). Episodes 39, 3–8.

Sperling, E.A., Frieder, C.A., Raman, A.V., Girguis, P.R., Levin, L.A., Knoll, A.H., 2013. Oxygen, ecology, and the Cambrian radiation of animals. Proceedings of the National Academy of Sciences 110, 13446–13451.

Sperling, E.A., Carbone, C., Strauss, J.V., Johnston, D.T., Narbonne, G.M., Macdonald, F. A., 2016. Oxygen, facies, and secular controls on the appearance of Cryogenian and Ediacaran body and trace fossils in the Mackenzie Mountains of northwestern Canada. GSA Bulletin 128, 558–575.

Sundvoll, B., Roberts, D., 2003. A likely early Ordovician age for the regional, penetrative cleavage in the Gaissa Nappe Complex, northern Norway. Norges Geologiske Undersøkelse Bulletin 441, 51–59.

Taillefert, M., Neuhuber, S., Bristow, G., 2007. The effect of tidal forcing on biogeochemical processes in intertidal salt marsh sediments. Geochemical Transactions 8, article number: 6. DOI:10.1186/1467-4866-8-6.

Taylor, S.R., McLennan, S.M., 1985. The Continental Crust: its Composition and Evolution. Blackwell, Oxford, p. 312.

Taylor, R.J.M., Clark, C., Harley, S.L., Kylander-Clark, A.R.C., Hacker, B.R., Kinny, P.D., 2017. Interpreting granulite facies events through rare earth element partitioning arrays. Journal of Metamorphic Geology 35, 759–775.

Tostevin, R., Mills, B.J.W., 2020. Reconciling proxy records and models of Earth's oxygenation during the Neoproterozoic and Palaeozoic. Interface Focus 10, article number: 20190137. https://doi.org/10.1098/rsfs.2019.0137.

Tostevin, R., Shields, G.A., Tarbuck, G.M., He, T., Clarkson, M.O., Wood, R., 2016a. Effective use of cerium anomalies as a redox proxy in carbonate-dominated marine settings. Chemical Geology 438, 146–162.

Tostevin, R., Wood, R.A., Shields, G.A., Poulton, S.W., Guilbaud, R., Bowyer, F., Penny, A.M., He, T., Curtis, A., Hoffmann, K.H., Clarkson, M.O., 2016b. Low-oxygen waters limited habitable space for early animals. Nature Communications 7, article number: 12818. DOI:10.1038/ncomms12818.

Vermeesch, P., 2018. IsoplotR: a free and open toolbox for geochronology. Geoscience Frontiers 9, 1479–1493.

Wallace, M.W., Hood, A.S., Shuster, A., Greig, A., Planavsky, N.J., Reed, C.P., 2017. Oxygenation history of the Neoproterozoic to early Phanerozoic and the rise of land plants. Earth and Planetary Science Letters 466, 12–19.

Wilde, P., Quinby-Hunt, M.S., Erdtmann, B.D., 1996. The whole-rock cerium anomaly: a potential indicator of eustatic sea-level changes in shales of the anoxic facies. Sedimentary Geology 101, 43–53.

Willbold, M., Jochum, K.P., 2005. Multi-element isotope dilution sector field ICP-MS: A precise technique for the analysis of geological materials and its application to geological reference materials. Geostandards and Geoanalytical Research 29, 63–82.

Wood, R.A., Poulton, S.W., Prave, A.R., Hoffmann, K.-H., Clarkson, M.O., Guilbaud, R., Lyne, J.W., Tostevin, R., Bowyer, F., Penny, A.M., Curtis, A., Kasemann, S.A., 2015. Dynamic redox conditions control late Ediacaran metazoan ecosystems in the Nama Group, Namibia. Precambrian Research 261, 252–271.

Wood, R., Liu, A.G., Bowyer, F., Wilby, P.R., Dunn, F.S., Kenchington, C.G., Hoyal Cuthill, J.F., Mitchell, E.G., Penny, A., 2019. Integrated records of environmental change and evolution challenge the Cambrian Explosion. Nature Ecology & Evolution 3, 528–538.

Zhang, F., Xiao, S., Romaniello, S.J., Hardisty, D., Li, C., Melezhik, V., Pokrovsky, B., Cheng, M., Shi, W., Lenton, T.M., Anbar, A.D., 2019. Global marine redox changes drove the rise and fall of the Ediacara biota. Geobiology 17, 594–610.

Zhang, W., Roberts, D., Pease, V., 2015. Provenance characteristics and regional implications of Neoproterozoic, Timanian-margin successions and a basal Caledonian nappe in northern Norway. Precambrian Research 268, 153–167.